Assessing the Long-Term Behaviour of the Industrial Bentonites Employed in a Repository for Radioactive Wastes by Studying Natural Bentonites in the Field

W. Russell Alexander [1,*], Heini M. Reijonen [2,3], Gillian MacKinnon [4], Antoni E. Milodowski [5], Alistair F. Pitty [6] and Andreas Siathas [7]

[1] Bedrock Geosciences, Veltheimerstrasse 18, 5105 Auenstein, Switzerland
[2] Geological Survey of Finland (GTK), P.O. Box 96, 02151 Espoo, Finland; heini.reijonen@gtk.fi
[3] Previous Address Saanio & Riekkoloa, Laulukuja 4, 00420 Helsinki, Finland
[4] Scottish Universities Environmental Research Centre (SUERC), Rankine Avenue, East Kilbride G75 0QF, UK; Gillian.Mackinnon@glasgow.ac.uk
[5] British Geological Survey (BGS), Nicker Hill, Keyworth NG12 5GG, UK; aem.amethystgeo@virginmedia.com
[6] Pitty (EIA) Consulting, Telegraph Lane East, Norwich NR1 4AN, UK; al.pitty2014@gmail.com
[7] Geoinvest, P.O. Box 20476, 2152 Aglantzia, Cyprus; geoinvest@cytanet.com.cy
* Correspondence: russell@bedrock-geosciences.com; Tel.: +41-76-531-3607

Abstract: Bentonite makes an important contribution to the performance of the engineered barriers in most radioactive waste repository designs. The choice of bentonite results from its favourable properties for waste isolation and its stability in relevant geological environments. However, the longevity of bentonite (especially the resistance to waste container sinking) has been little studied. Modelling results suggest significant bentonite deformation and associated canister sinking is unlikely and, here, long-term natural system data are used as a reality check on model predictions. Results indicate that bentonite from the investigated site shows no significant deviation in bulk physical parameters from repository bentonite. However, micro-scale shear planes can be seen throughout the sampled cores. The presence of multi-directional S- and C-type shears suggests they originate from loading from the overlying limestone, not gravitational tectonics. The plastic limits and angles of shearing resistance for natural and repository bentonites suggest both are susceptible to shearing. The impact of bentonite shear under load could be minimised by appropriate design, but existing lower activity waste container designs do not consider the potentially high external stresses from the bentonite backfill and this should be addressed in future.

Keywords: bentonite; waste canister sinking; shear displacement; reality check; engineering options

1. Introduction

Bentonite makes an important contribution to the performance of the engineered barrier system (EBS) and seals in most deep geological repository designs (see, for example, [1]). The choice of bentonite results from its favourable properties for isolation and containment of the waste (such as plasticity, swelling capacity, colloid filtration, low hydraulic conductivity, high retardation of key radionuclides) and its stability in relevant geological environments [2]. However, the longevity of bentonite—especially the potential for waste canister sinking/settling in bentonite (or bentonite-sand mixtures) over long timescales—has been little studied. Modelling suggests that it is unlikely, but this needs to be checked against data and the most appropriate method to do so is to utilise data from natural systems (where the relevant process has been operating for thousands to millions of years) as a "reality check" on model predictions of long-term processes [3–5]. To date, most modelling effort has

been focussed on the settlement of HLW (vitrified high-level waste) or SF (spent fuel) canisters [6] where the load on the bentonite is of the order of 0.1 to 0.2 MPa [7]. However, as various L/ILW (low- and intermediate-level waste) repositories worldwide move towards realisation [8], there is a requirement to assess the potential settlement of cementitious waste packages (Figure 1) and other structures and here the expected loads on the bentonite are greater, being in the order of 0.3 to 0.4 MPa.
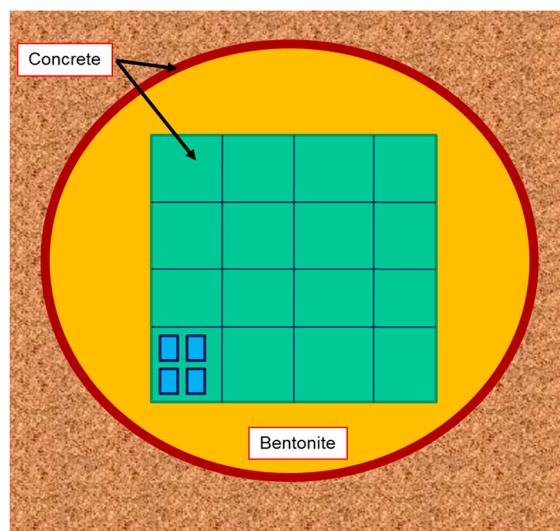

Figure 1. An example waste cavern design for a cementitious L/ILW (low- and intermediate-level waste) repository. Waste containers (**blue**, typically 200 L metal drums filled with waste and a cement grout) are encased in concrete boxes (**green**) which are usually backfilled with more cement grout. The boxes are then protected by industrial bentonite to minimise groundwater interaction with the waste. The tunnel walls may also be supported by concrete tunnel liners. From [9].

To date, the focus of work on bentonite settlement has been consolidation, with effectively only compaction of the bentonite below the waste package being of concern [10]. Generally, modelling simulations suggest this will be of negligible impact. However, more recent work indicates that creep-induced settlement could be of more concern. Consequently, the focus of this project was the assessment of the long-term performance of bentonite, in particular examination of potential lateral movement of bentonite under and around waste packages.

Argumentation by use of analogy is well established in many fields including philosophy, biology, linguistics and law [11]. For the specific case of radioactive waste management, the term "natural analogue" (NA) has developed a particular meaning associated with providing supporting arguments for the repository Safety Case (see, for example, [12] for discussion). Key factors here are the heterogeneity and complexity of natural systems and, in particular, the very long timescales over which safety must be assured. The potential evolution of repositories, designed for specific types of waste and disposal sites, can be simulated by the use of mathematical models, but the extent to which such models can be validated by conventional approaches is inherently limited. Here, natural (along with archaeological and anthropogenic) analogues—systems which have similar properties to components of repositories—have a unique role to play. The extent to which NA system evolution in the past can be understood and modelled with existing tools and data, gives an indication of the ability to determine future development of the repository.

The initial use of NAs focussed on improving understanding of key processes and model/database testing [13] and, indeed, this is still a major justification for some NA projects. More recently, however, additional roles in public communication [14] and staff training [15] have received greater emphasis. In particular, using natural analogues to provide general support for the safety case (by studying the evolution of relevant systems over geological timescales) and to increase confidence in extrapolating

results from laboratory and field experiments to the repository [3,16] have been a recent focus. This study most certainly belongs in this more recent domain.

Improving system understanding can range from examining global concepts (e.g., fundamental feasibility of preserving geochemical anomalies for millions of years—see discussions on the Oklo and Cigar Lake U ore bodies in [17]) to direct quantification of specific processes (e.g., rock matrix diffusion depths [18]). Similarly, model testing can range from rather weak qualitative comparison of expectations with observations (e.g., relative retention of elements within Oklo natural reactor cores [17]) to quantitative assessment of the relevance of laboratory databases (e.g., for material corrosion [19] Figure 2) to more formal assessment of the predictive capability of specific model and databases (e.g., blind predictive modelling of radionuclide solubility limits [20]).
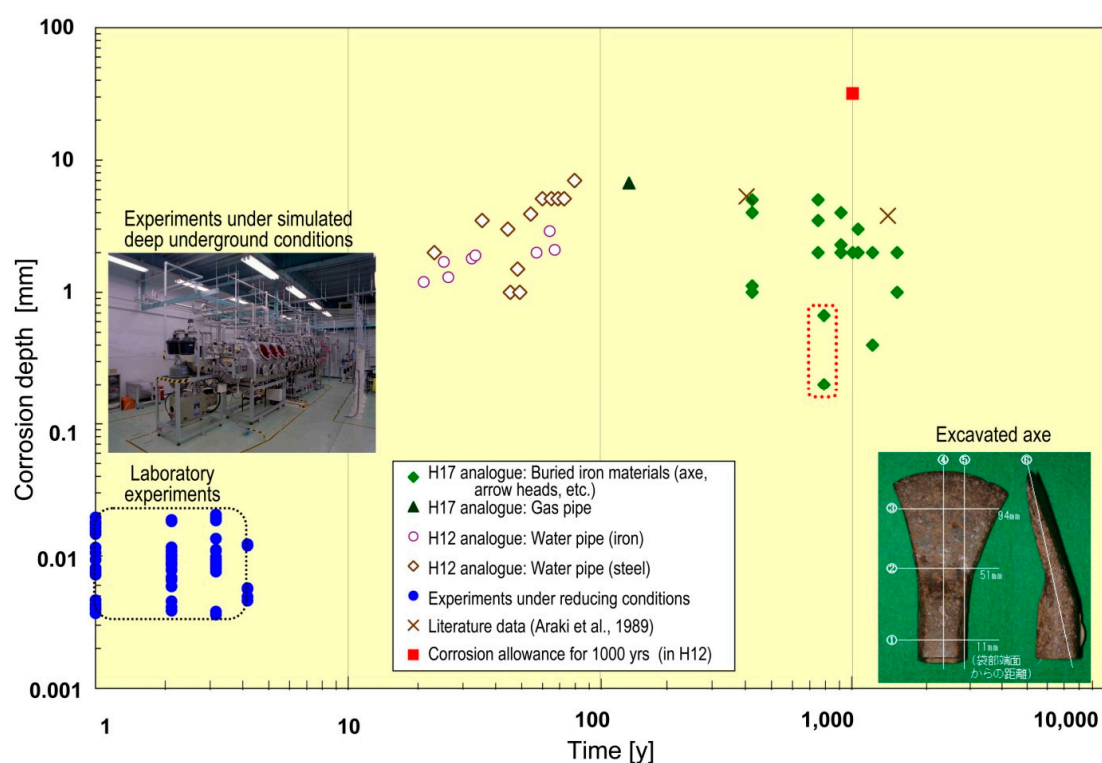

Figure 2. Integration of iron/steel corrosion data from laboratory experiments and several natural analogue sources (details in [19,21]). Note that the H17 analogues surrounded by the red dots are believed to have come from an aerobic environment.

The challenge is to maximise the value of tests such as shown in Figure 2 by assuring that materials and boundary conditions are as similar as possible to those in a repository. Nevertheless, it must be emphasised that such sites are no more than an analogy of a repository, not a copy and hence certain differences are inevitable. The natural bentonite is not a precise copy of the industrial bentonite which will be employed in a repository: it cannot be as an industrial bentonite is a natural bentonite which has then been treated to a range of artificial enhancements. For example, it may be processed (i.e., beneficiated) to improve the smectite content of the material and it can also be chemically treated to enhance its cation exchange, swelling or other physico-chemical properties (e.g., conversion or "activation" of natural calcium montmorillonite to sodium montmorillonite by treatment with sodium carbonate). Nevertheless, the basic material is the same and should, in most circumstances, behave similarly.

Overall then, of importance is the fact that, when compared with most existing studies of waste package settlement in bentonite, this study is the first to approach repository conditions insofar that the field conditions closely simulate what would be expected in a repository:

- an appropriately large mass of bentonite is "in place", rather than just a small plug of material within laboratory apparatus
- an appropriately dense overburden can settle into the bentonite in a manner similar to what would be expected in the repository EBS
- the settlement timescales are of much more relevance to a repository than accelerated laboratory and URL (underground research laboratory) studies
- potential chemical reaction between the overburden and the bentonite can be assessed. Generally, this is assumed to be diffusive transport of solutes (especially OH and Ca) into the body of the bentonite from the overburden/bentonite contact zone, again as would be expected in a repository where OH and Ca from the cementitious materials could interact with the bentonite
- the temperatures of reaction (ca. 10–30 °C) are also repository-relevant.

Consequently, it is the physical similarities between the appropriately dense limestone overburden/underlying natural bentonite and that expected in a repository EBS where a cementitious waste package could sink into the underlying (and enveloping, see Figure 1) bentonite which argues most strongly for studying long-term bentonite reaction in such natural systems—clearly indicating the relationship between engineered and natural barriers.

2. Geological Setting of the Study Area

The sampling site is located on a topographic high in a quarry to the southwest of Kato Moni village, on the northern flank of the Troodos mountain range in Cyprus (Figure 3). The Peristerona River, to the east of the site, is part of the Western Mesaoria Aquifer and current groundwater levels are low in the area.
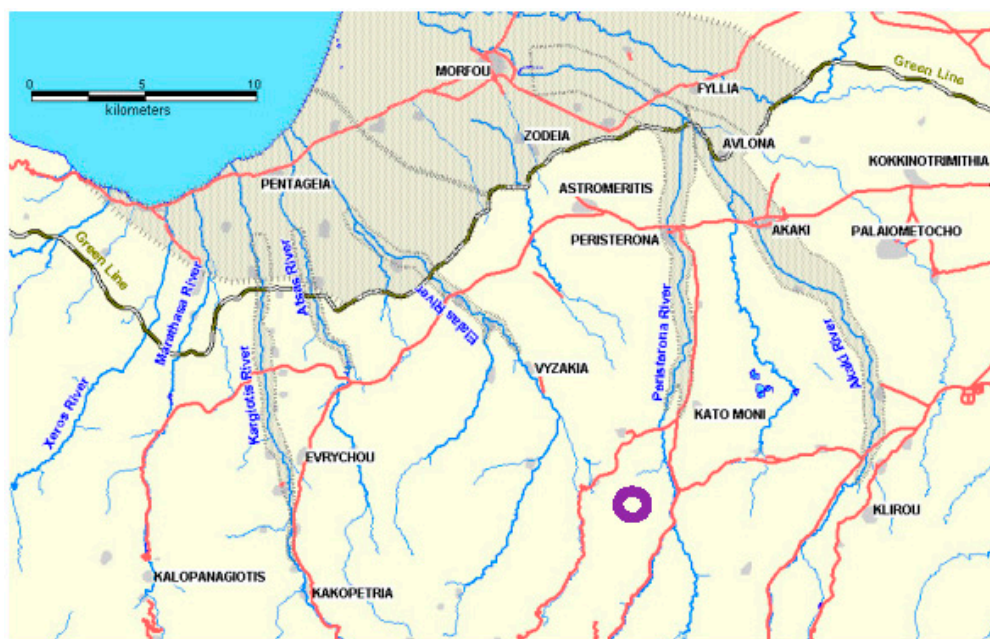

Figure 3. Location of the Kato Moni site (purple circle). After [22].

Geologically, the Kato Moni (KM) site lies on the northern edge of the Troodos ophiolite and a simplified geological map (Figure 4) of the KM area shows the following geological units:

- pre-Quaternary sedimentary cover (Lefkara, Pahkna and Nicosia Formations)
- Quaternary Fanglomarate Group to the north of the KM area
- in the channel area of the Peristerona River, Holocene alluvium deposits

In the area of Mesaoria, during the early Tertiary, the Lefkara formation was deposited over the ophiolite, followed by the deposition of the Pakhna formation [23]. The Mesaoria basin started to form towards the end of Miocene [24] and the Nicosia Formation is related to the filling stage of this graben.
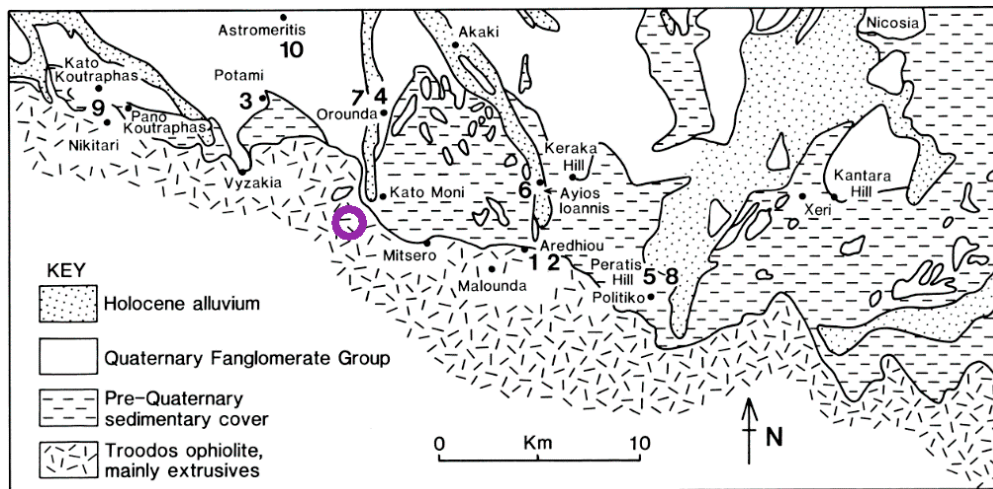

Figure 4. Simplified geological map of the study area (purple circle). From [25].

Limestone caprocks (generally present as topographic highs) are found throughout the area, directly overlying bentonite deposits and this is seen very clearly at the KM1 drilling site (see below). The massive bentonites (decametres thick), in turn, lie atop pillow lavas and umbers (manganese oxides). Bentonite colour varies from red to greenish gray and, on surface exposures, bentonite shows typical "popcorn" texture.

In the Kato Moni area, the limestones overlying the bentonite are from the Pakhna Formation and comprise of chalks and reef limestones [26]. The Pakhna Upper Miocene (Koronia Member) represents the second phase of reef growth on Cyprus. This later phase of reef growth is comparable with similar fringing reefs of monospecific, poritid coral reefs that were commonly developed around the Mediterranean basin in the Tortonian-early Messinian time. The morphology and distribution of the Koronia Member reef outcrops differ in each main area of exposure due to the fact that were controlled by local structural settings. The Koronia limestone is lithologically described as recrystallized bioclastic, bioherm and biostrom reefs. This dolomitic or magnesium-rich reef limestone has a creamy to off-white colour. The reef limestone that is exploited as a source of raw material for aggregates, is generally hard, massive and relatively porous whereas locally it may be bedded, brecciated and contain conglomeratic and/or sandy facies.

Limestones are generally white in the area while calcareous colluvium materials found, for example, on the northern side of the quarry show more red colouring than the limestone. Within this colluvial section, well rounded boulders are found, of which some represent lithologies found in the Troodos ophiolite (e.g., dunite). It appears that the rounded clasts are found in the upper part of this unit, while more angular, less heterogeneous, clasts dominate the lower unit.

Of the three boreholes drilled, KM1 penetrated 8.5 m of massive limestone before reaching the top of the bentonite. KM2 penetrated 2.5 m of blocky limestone followed by 7.2 m of red stained channel fill (of mixed limestone and ophiolite-derived boulders, cobbles and gravels) then 3.8 m of massive limestone before reaching the top of the bentonite at 13.5 m depth. KM3 was drilled directly on top of exposed bentonite. Geomorphological study of the KM area indicated that:

- as the Troodos Massif has been uplifted some 2000 m in ca. 2 Ma, the KM site has probably been exposed for around 0.5 Ma.
- average erosion rates of the limestone overburden could be in the order of 50 m in 1 Ma, suggesting local overburden loss at KM of some 25 m in that time.

- based on the likely main erosion processes onsite, it is suggested that the small valley in which the KM3 borehole was drilled was initiated at least 50 ka ago.
- it is also suggested that the valley sidewalls might retreat by some 6–12 m over a 10 ka time span, indicating that the valley bottom at the KM3 site has been exposed for a few ka at the very most, and possibly much less.

3. Materials and Methods

3.1. Field Sampling

The sampling site (Figure 5) was first cleared of the thin soil and scrub and partially levelled for rig access with a bulldozer before solid phase samples were collected by a combination of rock chip logging and coring. A Schramm Inc. (West Chester, PA, USA) rotary drilling rig and associated support equipment of Geoinvest Ltd. (Aglantzia, Cyprus) was used on site to drill four cored boreholes (Table 1). During testing/searching for lithological contacts, drill lubrication was air and samples were collected as rock chips during venting of the returned air from the borehole neck.
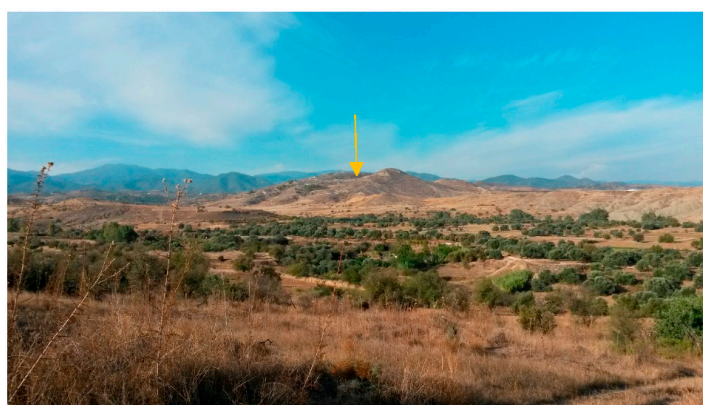

Figure 5. View of the KM site looking from the SSW. Yellow arrow showing the study area between the two topographic highs. Peristerona River valley in the foreground.

Table 1. Kato Moni borehole collar information (UTM/UPS WGS84 co-ordinate system).

Borehole ID	Eastings (°)	Northings (°)	Elevation (m.a.s.l.)
KM1	0506785	3880332	439
KM2	0506808	3880332	440
KM3a	0506844	3880391	425
KM3b	0506844	3880391	425

When an interesting feature was encountered, double barrel (i.e., steel outer core barrel with an inner plastic barrel to protect the samples—e.g., [27]) and, rarely, single barrel coring was employed along with a SPT split spoon sampler. But this could only be for a short duration due to overheating downhole which leads to complete baking of the bentonite samples. Instead, very slow drill rates and low WOB (weight on bit) with sparing use of water was employed to minimise disturbance to the bentonite samples.

Several good overviews of core handling methods are available in the literature [28,29] and, as far as was possible under the field conditions experienced, they were followed. Immediately upon recovery from the core barrels, the samples were wrapped in several layers of household plastic food wrap to minimise dessication. Following a very brief examination of the samples and core photography, the initial wrap was removed, the core sub-sampled (see Supplementary Materials Section S1) and the sub-samples were re-wrapped in food wrap and, to halt potential (load release related) expansion of

the core material, then further tightly wrapped in masking tape. The thus-wrapped samples were then placed inside small, rigid plastic boxes (with the void spaces filled with crushed paper to minimise movement during transport) which were taped tightly shut and then packed tightly in larger, rigid plastic boxes for transport to the various analytical facilities.

3.2. XRF/XRD

3.2.1. X-ray Fluorescence Analysis

A multi-element simultaneous X-ray fluorescence (XRF) analyser (Rigaku Simultix 14) was used in the elemental analysis. Analysis was carried out in full-width measurement mode by scanning goniometer.

3.2.2. X-ray Diffraction Analysis

X-ray diffraction analysis conformed to [30,31] and the analysis was carried out by using Shimadzu XRD-6100. All samples were powdered for analyses and four different sample types were produced:

- *Unoriented and untreated samples (all):* To provide an overview of the bulk sample mineralogy, unoriented and untreated samples were measured initially. After air drying at room temperature, all samples were ground in an agate mortar until smooth to the fingertip. The powdered samples were then loaded into the sample holder (aluminium plate depth 1mm diameter 25 mm).
- *Oriented and untreated samples (clay):* In order to identify the clay mineral composition in detail, oriented and untreated samples were measured. The above powdered samples were diluted with distilled water in a 300 mL beaker and, after standing for 4 h, the upper 5 cm (which is presumed to contain clay particles of less than 2 μm) was collected, centrifuged (1900 rpm, 10 min) and the resulting precipitate placed on a glass slide (two per sample) and then air dried.
- *Ethylene glycol treated samples (EG):* If peaks were identified near 10 Å or 14 Å in the oriented and untreated sample, the oriented samples were treated with ethylene glycol to determine if they represented smectite or chlorite. One set of oriented and untreated samples had a drop of ethylene glycol added and allowed to stand for about 5 min.
- *Hydrochloric acid treated samples (HCl):* If peaks were identified near 7 Å or 10 Å in the oriented and untreated samples, the oriented samples were treated with hydrochloric acid to determine if they represented kaolinite or chlorite. The above powdered samples were added to HCl (10 mL of 6 N) in a test tube and placed in a hot water bath for 120 min. Thereafter, they were centrifuged (1900 rpm, 5 min), the supernatant discarded and resaturated with distilled water. This was repeated five times and the final precipitate was then air dried on a slide glass.

3.3. Optical Petrographic Examination

Specific areas for thin sectioning were selected from each sample and impregnated with epoxy resin under vacuum to stabilise it during cutting and sectioning. A blue dye was added to the epoxy resin to enable any natural porosity to be readily identified during the subsequent optical petrographic examination. The target area on the resin-impregnated block was then cut using a diamond-tipped saw. The blocks were mounted onto glass slides with colourless epoxy resin and ground to produce polished (48 × 28 mm) thin sections to a standard thickness of 30 μm. Large format sections (78 × 50 mm) were made from five of the samples. All grinding and polishing of the sections was carried under ethanol, rather than water-based lubricants, in order to prevent reaction and swelling with the water-sensitive smectite present in the bentonite samples. The polished sections were examined by optical microscopy under plane-polarized light (PPL) and cross-polarized light (XPL) condition.

Backscattered scanning electron microscopy (BSEM) was used to make detailed high-resolution petrographical observations of the polished thin sections. BSEM analyses were carried out using a FEI QUANTA 600 environmental scanning electron microscope (ESEM) fitted with an Oxford Instruments

INCA Energy 450 energy-dispersive X-ray microanalysis (EDXA) system with an Oxford Instruments X-MAX 50 mm^2 Peltier-cooled (liquid nitrogen free) silicon drift detector (SSD). The polished sections were coated with a nominally 25 nm thick film of carbon, prior to examination in the ESEM instrument (high vacuum mode, with a routine electron beam accelerating voltage of 20 kV, and beam probe currents of between 0.71 and 1.2 nA, and a working distance of 10 mm) to make them electrically-conductive. Carbon-coating was carried out using an EMITECH 960 L evaporation-coating unit. Mineral/phase identification was aided by micro-chemical information routinely obtained from simultaneous observation of semi-quantitative EDXA spectra recorded from features of interest. EDXA data was acquired and processed using the Oxford Energy INCA Suite Version 5.04 Issue 21a+SP2 (2012) software package. In addition, quantitative electron microprobe analysis was also performed on selected polished sections by SEM EDXA.

3.4. Bentonite Physical Properties

The laboratory tests at Geoinvest were performed in accordance with [32,33] and involve identification tests, strength tests, swelling and clay surface area as follows:

- *Natural Moisture Content*: All natural moisture content tests, in accordance with [34], were determined for all samples tested for Unconfined Compressive Strength, as well as for samples tested for Atterberg Limits.
- *Specific Gravity/Particle Density*: This test was carried out in accordance with [35].
- *Bulk and Dry Density*: These tests were carried out in accordance with [36].
- *Atterberg Limits*: Testing was carried out in accordance with the requirements of [37]. The Cone penetration apparatus (method 2B) was adopted for the liquid limit tests. The results are presented graphically on individual test sheets and on the Casagrande Plasticity Classification Chart. All samples tested for Atterberg Limits were also tested for linear shrinkage.
- *Unconfined Compression Tests*: Eighteen Unconfined Compression tests were carried out on cored samples on the ELE-MULTIPLEX 50 triaxial machine. The treatment and testing of samples was in accordance with [38]. The orientation of the samples when placed in the testing machine was as in situ and the rate of strain applied was 1.00 mm·min^{-1}.
- *Triaxial Strength Tests*: The Unconsolidated Undrained Triaxial Tests (UU) were carried out at various cell pressures in accordance with the requirements of [39] in order to obtain values of the peak strength, cohesion and angle of shearing resistance (total values).
- *Swelling Pressure*: The testing was performed in accordance with the procedure given in [40]. They are presented graphically with the cumulative weight vs. square root of time.

3.5. Cation Exchange Capacity (CEC) and Exchangeable Cation Composition (EC) Analysis

3.5.1. Ba—Mg Compulsive Exchange Method for CEC

Ammonium and barium ions are commonly used as index cations for the determination of CEC in geological materials, but the ammonium exchange method is laborious and can be problematic [41] and because it involves reaction with ammonium acetate solution buffered to pH 7, it can be prone to errors caused by the dissolution of calcium carbonate minerals. Since calcite and gypsum were expected to be potentially present in the bentonite analogue deposits from KM, the CEC of the samples was therefore determined using the technique based on the compulsive exchange between an aqueous solution of magnesium sulphate and a barium soil [42,43]. The CEC was determined as the equivalent cation charge per unit mass, corresponding to the amount of magnesium exchanged.

3.5.2. EC Analysis

Exchangeable cation (EC) contents were determined by ICP-AES analysis of the combined barium chloride/triethanolamine extractant solutions recovered from the first stage of the CEC analysis.

The ICP-AES analyses were calibrated against matrix matched standards and carried out using a Perkin Elmer Optima 7300 DV dual view spectrometer fitted with a echelle polychromator and a UV/vis solid state segmented-array charge-coupled device detector with continuous wavelength coverage from 165 to 782 nm.

3.6. Stable Isotopes

A minimum of 10 mg of carbonate (calcite) material was extracted for each of the samples identified for stable isotope analysis. This material was carefully scraped (as a powder) from the sample onto clean paper, using a stainless steel scalpel blade, and then placed in a 2 mL Eppendorf Safelock® microcentrifuge tube for storage prior to analysis. Approximately 10 mg of the bulk powdered calcite (i.e., bulk limestone, diagenetic calcite cement or calcite fracture filling) was used for isotope analysis using a GV IsoPrime mass spectrometer plus Multiprep device. Isotope values ($\delta^{13}C$, $\delta^{18}O$) are reported as per mille (‰) deviations of the isotopic ratios ($^{13}C/^{12}C$, $^{18}O/^{16}O$) calculated by reference to the Virtual Pee Dee Belemnite (VPDB) scale, using a within-run internal laboratory (BGS) secondary standard (BDH calcium carbonate) that has been calibrated against the NBS Magcobar Calcite standard. Analytical precision is <0.1‰ for $\delta^{13}C$ and $\delta^{18}O$.

3.7. Natural Decay Series (NDS)

3.7.1. Alpha Spectroscopy

A sub-sample (~2.0 g) of each powdered rock was heated in a furnace to remove organic material after which 1 mL of ^{232}U in transient equilibrium with ^{228}Th was added as a yield tracer (Atomic Energy Harwell, AE 1943/2a, ^{232}U diluted activity: 0.162 Bq·mL^{-1}). Samples underwent dissolution in a series of aqua regia (1 HCl:1 HNO$_3$), H$_2$O$_2$ and HF as required until all remnants of rock were dissolved and no residue remained. The samples were then leached with 4 M HNO$_3$, ready for purification and separation of U and Th based on the method of [44].

Electrodeposition of U and Th for alpha spectroscopy: both U and Th were electrodeposited in the same way. Each fraction was first dried and then dissolved in a few drops of 1.2 M HCl, after which 30 mL of plating solution (3.75% ammonium chloride) was added. Each fraction was then introduced to an individual plating cell, ensuring that the electrode was positioned centrally over the stainless steel planchette. Samples were then plated for ~1.5 h at a current of 3 amps. Once electroplating was complete, the planchettes were dried and transferred to an Ortec Octete Plus alpha spectroscopy system and alpha spectra were recorded for approximately 1 week.

3.7.2. Gamma Spectroscopy

The samples were analysed by gamma spectroscopy, using a uniform sample weight of 20 g of the same dried, powdered rock sub-sample as was used for the alpha spectroscopy. Samples were placed in plastic containers to provide an uniform geometry and positioned in a reproducible manner on the end face of a High Purity intrinsic Germanium (HPGe) gamma photon detector. The detector used was an EG&G Ortec LO-AX series HPGe Low-Energy detector with a low background cryostat configuration, resolution of 601 eV (FWHM at 122 keV, Co-57) housed in a 10 cm Pb shield with a graded Cd/Cu lining to give a suitably low background. Spectra were corrected for background contribution. Analysis times of 96–168 h were used to obtain appropriate counting statistics uncertainties. Detection efficiencies were established using internationally accredited reference materials (IAEA gamma spectrometry reference materials, RGU-1 and RGTh-1).

3.8. Smectite Content Estimation Utilising the Methylene Blue Method

Methylene blue tests performed by Geoinvest were done in accordance with the procedure given in [45].

4. Results

4.1. XRD/XRF

4.1.1. XRF

The full extracted qualitative data set is presented in Supplementary Materials Section S2 and the data are plotted in Figures 6–8 for core samples from boreholes KM1, KM2 and KM3 respectively.
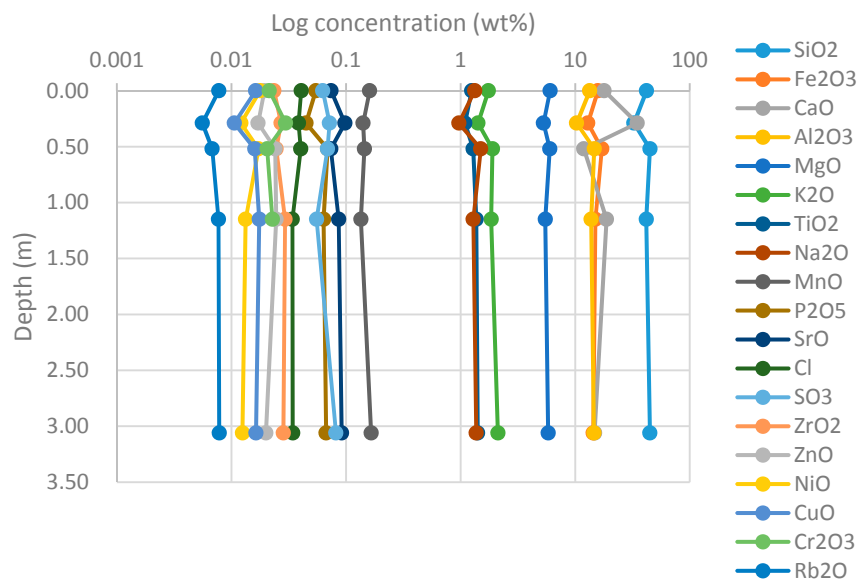

Figure 6. X-ray fluorescence (XRF) data for bentonite in borehole KM1 (normal-log plot). All depths are from the base of the overlying limestone.
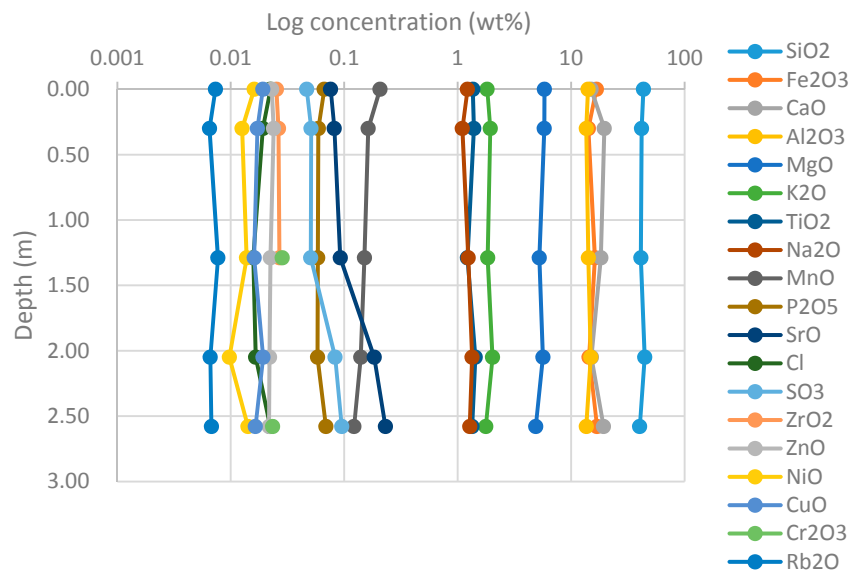

Figure 7. XRF data for bentonite in borehole KM2 (normal-log plot). All depths are from the base of the overlying limestone.
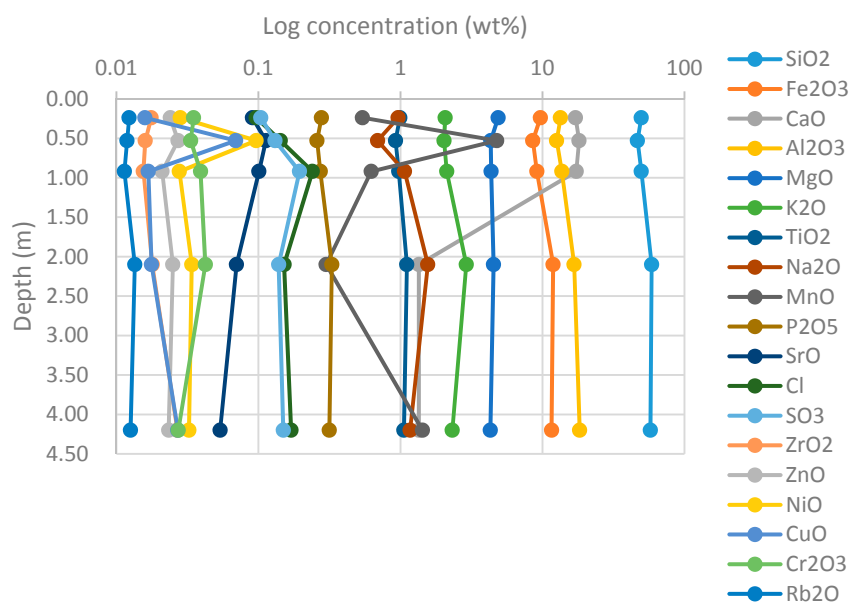
Figure 8. XRF data for bentonite in borehole KM3 (normal-log plot). All depths are from the base of the overlying limestone.

In Figure 6, it is clear that there is a co-related variation in the concentrations of Ca and Si/Al/Fe in core KM1, with this being particularly pronounced in the top metre or so. This would suggest a co-variation in carbonate and detrital silicate minerals. That the Sr concentration also increases sympathetically with Ca would support this assumption. Similarly, P (as an analogy for detrital apatite) and other aluminosilicate mineral associated elements (e.g., Na, K, Ti) also decrease with Si, Al and Fe. Otherwise, there is little variation with depth in KM1.

In core KM2 (Figure 7), there is a similar co-variance throughout, even if the magnitude is not as great as in KM1. Interestingly, in Section 4.4 (CEC), it is noted that part of the "excess" Ca in some areas of the cores may represent gypsum and, to some extent, the S trends are similar to that of Ca (and Sr). However, as the absolute values of S are several orders of magnitude lower than that of Ca, it is unlikely that gypsum represents more than a very small proportion of the Ca inventory in these bentonites.

In core KM3 (Figure 8), the major element pattern is similar to that in core KM1 with what is likely to be the same carbonate/detrital silicates covariance indicated (Figure 6). Of note also is the Mn peak at 0.5 m depth in KM3 which is an order of magnitude enriched over the core "background" concentrations. This is likely due to some localised umber (metal-rich clays) concentrations nearby in the quarry, lying atop the pillow lavas. In some bentonites, for example at the Saile site in Luzon [15] or Parsata in Cyprus [9] such bedding-controlled, Mn-enriched horizons are commonplace.

Of further interest is the Cl peak near the surface of KM3 which is presumably of saline origin. Unfortunately, it is not possible to comment further on potential marine sources of the Cl as it cannot be cross-correlated with Na due to it's 5–10 times higher concentration in the core samples (the signal is presumably swamped by the Na in the clays). In other words, a situation not dissimilar with that of the possible marine gypsum input mentioned above and in Section 4.4. But there is a strikingly similar relation between the Cl and S concentrations in core KM3, suggesting at least some gypsum input to the site, possibly from the overlying Messinian Salinity Crisis sediments nearby.

4.1.2. XRD

The full extracted qualitative data set is presented in Table 2. These results are merely qualitative as can be seen from the fact that the methyl blue adsorption data (Section 4.4.2) indicate smectite contents of 20%–36%.

Table 2. Qualitative X-ray Diffraction Analysis (XRD) results for the Kato Moni boreholes KM1, KM2 and KM3.

Sample		Smec-Tite	Mica	Kaol-Inite	Laumontite	Quartz	Plagioclase	Aragonite	Ankerite	Calcite	Pyrite
KM1	B1sub	△		▪		△	◎			△	
KM1	B2sub	▪	▪	▪ (※1)		▪	△			◎	
KM1	B3sub	△	▪ (※1)	▪		△	△			△	
KM1	B4sub	△	▪ (※1)	▪		▪	△			○	▪ (※2)
KM1	B7sub	△	▪ (※1)	▪	▪	△	△			△	
KM2	B1sub	△	▪ (※1)	▪		▪	△			△	
KM2	B3sub	△	▪ (※1)	▪		△	△			△	
KM2	B4sub	△	▪	▪		△	△			△	▪ (※2)
KM2	B6sub	△	▪ (※1)	▪	▪	△	△	▪		△	▪ (※3)
KM2	B7sub	△		▪		△	△	▪		△	▪ (※3)
KM3	B1sub	△	▪	▪ (※1)	▪	△	▪		▪	○	
KM3	B2sub	△	▪	▪ (※1)	▪	△	▪		▪	○	
KM3	B3sub	○	▪	▪ (※1)	▪	△	▪		▪	△	
KM3	B5sub	○	▪	▪	▪	△	△				
KM3	B7sub	○	▪	▪	▪	△	△				

Key: ◎: Abundant; ○: Moderate; △: Scarce; ▪ : Rare; ※1 Elutriation only; ※2 Only one peak; ※3 Overlapping with aragonite.

4.2. Optical Petrographic Examination

4.2.1. Petrography of Boreholes KM1, KM2 and KM3

As so much material was analysed, sample-by-sample details are provided in Supplementary Materials Section S3 and, below, a summary of the key findings by borehole is given.

KM1 and KM2 are similar in most aspects and so will be treated together here. Both boreholes are capped with an argillaceous, micritic limestone. Some secondary calcium carbonate recrystallisation is present within fractures in the limestone samples due to remobilisation and re-precipitation of the original micritic calcium carbonate. All limestone samples from these boreholes are fractured and, in general, fractures were angular, clean, pull-apart fractures (e.g., sample KM1 B6, Supplementary Materials Section S3) so were assumed to be predominantly from drill damage. Element mapping indicates little in the way of secondary precipitation or alteration along any of the fractures apart from rare, minor Fe mobilisation.

The remainder of both boreholes primarily comprises fine-grained smectitic clay, although some variation in grain size was observed within the samples with the coarser grained material contained a higher porosity than the fine-grained material. Micro-fossil content is rich in some samples such as KM1 B1, B2a and B4 (see Supplementary Materials Sections S1 and S3) and micro-fossils/fossil fragments are present in most samples within the boreholes.

The bentonite clay matrix was analysed by EDXA to determine the clay mineral chemistry. These data were plotted as APFU values on triaxial plots to explore potential compositional variations. The results are presented as SiOI (Figure 9) and AFM (Figure 10) triaxial plots (see Figures S1 and S2 in Supplementary Materials Section S3 for borehole KM2). The SiOI plot shows there is a range in octahedral cations, from ~25% to 43%. The mean composition plots close to the end member composition of montmorillonite and the overall data are clustered around both the montmorillonite, and sepiolite-talc end-member compositions. The data in the AFM plot show a large Al variation, with most analyses ranging between 40% and 70%. Much of this variation is almost certainly due to the EDXA analyses representing mixtures of minerals in the clay matrix. However, overall, the data suggest the clay compositions lie between two dioctahedral smectite end members: montmorillonite and beidellite.
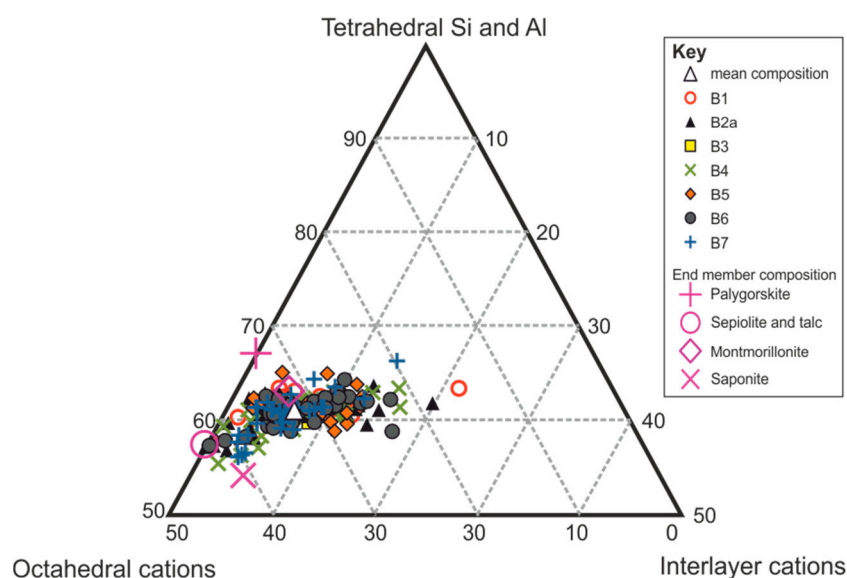

Figure 9. Borehole KM1 triaxial Si—octahedral cations—interlayer cations plot using APFU values. All clay data colour-coded by sample. End member palygorskite, sepiolite, talc, montmorillonite and saponite points included for reference.
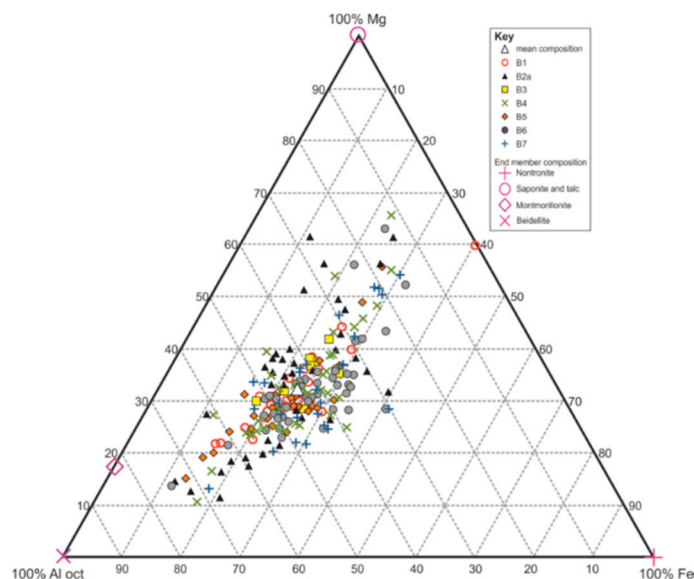
Figure 10. Borehole KM1 triaxial octahedral Al–Fe–Mg cations plot using atoms per functional unit (APFU) values. All clay data colour coded by sample. End member nontronite, beidellite, talc, saponite and montmorillonite points included for reference.

In borehole KM3, the APFU and AFM triaxial plots (see Figures C3 and C4 in Supplementary Materials Section S3) indicate that the compositional range is more tightly clustered and shows less variation than both KM1 and KM2. The mean composition plots close to the end member composition of montmorillonite, and the overall data are clustered around this end-member point. The data are also less scattered in the AFM plot, showing an Al range of 32%–89%. Overall the clay mineral chemistry appears to lie between the two dioctahedral smectite end member compositions: montmorillonite and beidellite.

4.2.2. Bentonite Texture

Detailed descriptions of the petrography and micro-fabric for individual samples of the Kato Moni bentonite are provided in Supplementary Materials Section S3 and the Plate numbers mentioned here refer to the Plates in S3.

The bentonite samples from all three boreholes (KM1, KM2 and KM3) display micro-fracturing. As noted in Section 3.1, steps were taken to minimise drilling and sub-sampling induced damage to the samples, but it must be emphasised that at least some of the fracturing observed in some samples may have been induced (or enhanced) as a result of the coring and sample preparation process. This is particularly evident from the significant deformation of bedding, caused by the dragging of the bentonite core along the inside of the core barrel, observed in samples KM2-B3 (Plate C46), KM3-B3 (Plate C88), KM3-B4 (Plate C94) and KM3-B7 (Plate C115).

In the case of sample KM1-B1, the material was already completely fractured and disaggregated on arrival at the analytical laboratory due to damage during transport. In addition, the subsequent preparation of thin sections for petrographic analysis required the samples to be dried prior to the material being impregnated with epoxy resin (a pre-requisite for thin section manufacture). Inevitably, this process will have caused some drying-shrinkage of these water-sensitive, smectite-rich sedimentary rocks, which in turn will have induced some of the tensional ("pull-apart") micro-fracturing that was observed in the thin sections.

Sample shrinkage and fracturing induced by sample drying might be reduced by use of a sophisticated solvent-replacement technique for thin-section preparation. This technique involves the slow-diffusive replacement of porewater in the sample by a water-miscible solvent (e.g., acetone or

propan-2-ol), which in turn is diffusively-replaced by a solution of resin in the solvent [46]. The resin is then cured by allowing the solvent to evaporate. This methodology has previously been used very successfully to minimise drying-induced artefacts in petrographic studies of water-sensitive soils and unconsolidated sediments [47], and in the analysis of glacio-tectonic fabrics in clay-rich sediments [48]. Unfortunately, this thin section preparation technique is very time consuming; the diffusive solvent-replacement process can take 6 to 12 months for completion, depending on the permeability of the material.

In general, the fracturing in bentonite from boreholes KM1 and KM2 displayed broadly similar characteristics. Most fractures were angular, clean, unmineralised, tensional pull-apart structures. The microfractures often deviate around the boundaries of coarse grains. Much of this type of fracturing shows no evidence for displacement of the bentonite across the fractures (i.e., no shear component). Similarly, there is no evidence for mineralogical alteration along these features. As discussed above, at least some of these fractures must have been induced as tensional micro-fractures possibly from relaxation after retrieving the core and/or from drying and shrinkage of the bentonite during the thin-sectioning process.

Fine banding is observed in some samples from boreholes KM1 and KM2 and it may represent primary sedimentary bedding lamination. This sedimentary fabric impacts on the deformation and fracturing behaviour of the bentonite as, where the banding or lamination is present, the bentonite displays intense micro-fracturing oriented parallel to the lamination. A marked difference was observed in the geometric characteristics between the fracturing found in the coarser and finer bands. In general, fractures displayed a more irregular or sinuous morphology in coarser grained bands, whereas the finer bentonite bands displayed fracturing that was characterised by tensional "pull-apart" fractures. The differences in fracturing behaviour are interpreted to be due to differences in the heterogeneity and physical properties between the coarser and finer layers. The finer layers are characteristically more uniform and, being clay-rich, will have a higher smectite content than the coarser silty layers. As such, they are likely to behave in a more plastic, rather than brittle, manner.

In addition, having a high smectite content, is likely to result in them having a greater propensity to producing tensional "pull-apart" shrinkage cracks on drying. In contrast, the coarser, siltier laminae are more heterogeneous, with fracturing being deflected around the boundaries of more competent clasts and grains, producing a more sinuous fracture trace. Also, having lower clay (smectite) contents, the coarser bands are less susceptible to shrinkage by sample drying during transport and thin section preparation. In both cases, the dominant fracture orientation tends to be sub-parallel to bedding, which is consistent with shrinkage perpendicular to the sedimented clay particle orientation. As before, no evidence of mineralogical alteration along these laminae was observed.

Some samples displayed evidence of natural fracturing, associated with shear displacement. In particular, sample KM1-B5 (Plates C30–C34) showed evidence for the formation of steeply-included tensional fractures that were offset on a millimetre-scale by shear along denser bedding-parallel bentonite seams (Figure 11). Some samples, for example KM1-B6 (Plates C38–C40) and KM1-B7 (Plates C43–C45), showed the development of micro-fracturing around the boundaries of discrete "clots" of bentonite. These were stained or mineralised by fine-grained secondary iron oxide, which indicates that they had formed in situ. It seems likely that these fractures therefore originated as shrinkage cracks during "drying" of the bentonite in situ. Sample KM1-B6 also displayed the development of a network conjugate, steeply-inclined, micro-faults (cf. Figure 12).
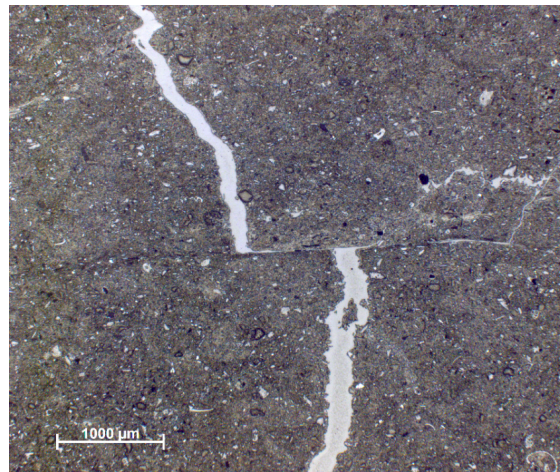
Figure 11. Reflected light image shows how a fracture has moved en-echelon along a thin, dense, horizontal seam in sample KM1 B5 (Plate C32 from Supplementary Materials Section S3).
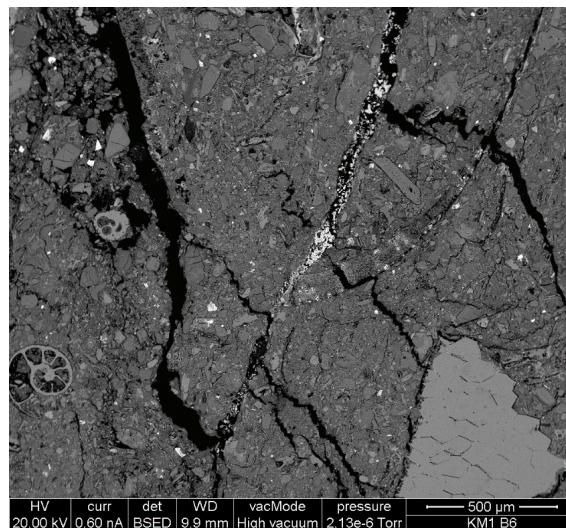

Figure 12. BSEM image of some of the major faults within sample KM1 B6. Most here form a network of straight conjugate faults, but a curved listric fault crosses the centre of the image (Plate C39 in Supplementary Materials Section S3).

Some of these micro-faults displayed listric surfaces that "tailed off" into shear surfaces propagating along bedding lamination. These were seen to be mineralised by fine-grained secondary iron oxide, which demonstrated that these were natural features in the bentonite and had not been produced by coring and subsequent sample preparation.

For boreholes KM1 and KM2, the most significant points are:

- if the sampling induced "drying", pull-apart features are ignored, the pattern of faulting indicates that there has been some lateral shear along the bedding planes.
- in most cases, the sense of shear is unclear, so it is not possible to define if the shear is an accommodation of compressive stress by movement on foliation planes—or simply a response to gravitationally-induced movement towards the local valleys around the Kato Moni quarry.
- more importantly, there is evidence of some multi-directional shear in the bentonite. The network conjugate, steeply-inclined, micro-faults that tail-off into shear fabrics suggest movement in at least two directions—i.e., movement unlikely to be gravitationally induced.

The samples from borehole KM3 displayed markedly different fracturing characteristics to that seen in KM1 and KM2. Samples from the top of KM3 are highly fractured and can be described as "pulverised" as exemplified by samples KM3-B1 (Plates C78–C81), KM3-B2 (Plates C84–C87) and KM3-B3 (Plates C90–C93). With depth, these pass through a transition interval with the development of an intact "chicken-wire" network of micro-fractures or a "pelletised" micro-fabric seen in samples KM3-B4 (e.g., Plate C96) to KM3-B7 (e.g., Plate C120). The fractures in this "chicken-wire" fabric are defined by anastomising shear plane networks (e.g., sample KM3-B4, as noted above). Much of this fracturing may be, at least partially, influenced by the original sedimentary fabric in the bentonite, and appears to pick out the boundaries of what may represent a primary pelletised mudstone fabric (e.g., sample KM3-B5, Plates C104 and C105). Such a pattern could be produced by a lapilli tuff (or, in this case, a micro-lapilli tuff) and bentonites produced by such lapilli falls have recently been identified elsewhere [49].

Towards the bottom of the borehole (sample KM3-B7), the fracturing in the bentonite displays well-developed shear fabrics, that are typified by well-defined "erring-bone"-like S- and C-type shear fabrics. Some of the minor secondary carbonate formed along these features in sample KM3-B3.

For borehole KM3, two points are of significance:

- as in boreholes KM1 and KM2, there is evidence of multi-directional shear in the bentonite, only it is more clear in KM3. The S- and C-type shear fabrics present here clearly indicate movement in at least two directions, with the shear zone representing an accommodation of compressive stress by movement on foliation planes (cf. [50]).
- the "chicken wire" network has already been proposed as an analogue of industrial bentonite pellets [49] due to similarities in form between lapilli tuff sourced bentonite and the industrial bentonites. That the shear plane networks are of a different form to those propagated in the more homogenous bentonite of boreholes KM1 and KM2 suggests that these features would be worth further study to assess if the fundamental shear process is different in bentonite pellets. For example, is the load of the overlying limestone being dissipated in a different form due to the pellet structure? That the S- and C-type shear fabrics "reappear" in borehole KM3 at depth when the bentonite fabric is once more homogenous suggests this to be the case.

4.3. Bentonite Physical Properties

The range in values of the analyses are presented in Table 3 and the full dataset is presented in Supplementary Materials Section S4.

Table 3. Range of physical properties of bentonite from cores KM1, KM2, KM3 and KM3a.

Atterberg Limits			UCS				Sp Grav.	Sw Press (kPa)	UU Triaxial	
PI (%)	Shrinkage (%)	MC (%)	MC (%)	BD (g/cm^3)	DD (g/cm^3)	qu (kPa)			Cohesion (kPa)	φ°
62–132	37–103	14–29	21.4–34.3	1.34–1.92	1.09–1.58	174–581	2.499–2.861	109.8–367.3	25–205	9–22

It can be seen from Table 4 that, despite the non-processed nature of the natural bentonite, most of the parameters fall within or are close to Posiva's guideline values for the (processed) industrial bentonite where it is noted that the main functional properties of the industrial bentonite in the EBS are:

1. Low hydraulic conductivity
2. Sufficient swelling pressure
3. Workability
4. Sufficient density
5. Sufficient thermal conductivity

Only in swelling pressure, itself a reflection of the low smectite content of the natural bentonite, is there a significant deviation with the natural bentonite displaying a much lower capacity to swell than the industrial bentonites. Indeed, the swelling pressures are more comparable with a mixture of industrial bentonite and crushed rock (Table 5).

Table 4. Values for some selected physical parameters of the Kato Moni natural bentonite compared with other natural bentonites from Parsata in Cyprus and example industrial bentonites from the Finnish SF programme (values at emplacement in the repository).

Parameter	Dry Density (kg· m^{-3})	Water Content (%)	Smectite Content (%)	Liquid Limit (%)	Plastic Limit (%)	Plasticity Index	CEC mEq (100 g^{-1})	Swelling Pressure (MPa)
natural Ca-bentonites								
KM1-B6-3	1410–1460	28.8	20.6–27.3 [1]	84	25	59	50.75 [2]	0.20
KM2-B3-2	1550	23.5	29.1 [3]	113	20	93	46.95	0.19
KM3a-B5-3	1230	34.2	26.6–36.2 [4]	112	32	80	55.95 [5]	0.34
T5 [6] (Parsata)	1340–1390	17–23	24–28	106–131	39–49	67–95	34–43	0.12–0.17
industrial Na-bentonites								
Posiva SF rings [7,8]	1752	17	>75	>80			>60	
Posiva SF disc blocks [7,8]	1701	17	>75	>80			>60	
Posiva SF pellets [7,8]	919	17	>75	>80			>60	
Posiva buffer Ca-bentonite [9]		13–15	65-≥75	60-≥80	50	10-≥30	50-≥60	≥2
Posiva buffer Na-bentonite [9]		13–15	65-≥75	200-≥250	50	150-≥200	60-≥70	≥2
Kunigel-V1 [10]	2790		48	473.9	26.61	447.3	73.2	
MX-80 [10,11]	2880		80	437.3	38.0	399.3	110.4	7.3 [12]
NEO-KUNIBOND [10,11] industrial Na-bentonite	2680		76	607.5	50.69	556.8	103.5	
KUNIBOND [1,10] industrial Ca-bentonite	2.71		84	128.7	38.4	90.3	79.5	

[1] average of 7 measurements from borehole KM1, calculated from methylene blue values (see Supplementary Materials Section S4); [2] sample KM1-B7 (see Supplementary Materials Section S1); [3] 1 measurement from borehole KM2, calculated from methylene blue values (see Supplementary Materials Section S4); [4] average of 10 measurements from boreholes KM3a and KM3b, calculated from methylene blue values (see Supplementary Materials Section S4); [5] sample KM3a-B4 (see Supplementary Materials Section S1); [6] [9]; [7] [51]; [8] [52]; [9] [53]; [10] [54]; [11] [55]; [12] [56].

Table 5. Comparison of physical parameters for the Kato Moni and Parsata natural bentonites and MX-80 industrial bentonite and mixtures of crushed rock and montmorillonite-rich clay (data for MX-80 and GEKO industrial bentonites from [56]).

Bentonite	Kato Moni KM3a	Parsata	MX-80	MX-80	GEKO/QI	MX-80	GEKO/QI
% clay	26–33	24–50	100	50	30	30	10
Density (at water saturation) kg·m^{-3}	1340–1700	1600–1680	2000	2100	2200	1950	2200
Swelling pressure (MPa in distilled water)	0.15–0.34	0.09–0.17	7.3	2.0	0.9	0.2	0.1

4.4. CEC and Methyl Blue Adsorption

4.4.1. CEC

The cation exchange capacity (CEC) and exchangeable cation (EC) chemistry, including total exchangeable cations (Σ) anlyses are presented in Table 6. The CEC values of the bentonite samples range from 43.60 meq 100 g^{-1} to 57.53 meq 100 g^{-1}. There is very little difference in CEC between samples from boreholes KM1 and KM2, although samples of bentonite from KM3 generally appear to have a slightly higher CEC.

The EC chemistry of most of the Kato Moni bentonite samples is dominated by Ca, with minor Mg and Na. Trace amounts of Sr, Mn and Fe were also measured during the exchangeable cation extraction, but K is below detection in most cases. The results present in Table 6 show a very large discrepancy between the CEC measured by the barium chloride displacement method [42] and the total of exchangeable cations (Σ) measured by ICP-AES. The Σ values are considerably greater that the measured CEC values in most cases. However, most of the excess cationic charge in the Σ value from ICP-AES, relative to the CEC measured by barium chloride displacement, appears to be due to the very high Ca content determined by ICP-AES. Samples KM3-B4 and KM3-B7 are anomalous in this respect: the CEC and Σ values for these two samples are much closer. This coincides with the much lower exchangeable Ca content exhibited in these two samples.

Table 6. Summary of cation exchange capacity and exchangeable cation chemistry for cores KM1, KM2 and KM3.

Sample	Depth (m)	CEC (meq 100 g^{-1})	Exchangable Cations (meq 100 g^{-1})							
			Ca	Mg	Na	K	Sr	Mn	Fe	Total Exchangeable Cations (Σ)
KM1										
KM1 B1	8.55	50.89	291.5	29.9	10.4	nd	0.50	0.03	0.26	332.6
KM1 B2a	8.77	43.60	373.4	27.4	8.1	nd	0.50	0.03	0.23	409.6
KM1 B3	9.00	53.01	267.0	30.6	10.3	nd	0.54	0.05	0.32	308.8
KM1 B4	9.60	53.20	303.6	34.1	10.7	nd	0.58	0.06	0.24	349.3
KM1 B7	11.55	50.75	299.4	31.5	10.8	nd	0.68	0.07	0.23	342.8
KM2										
KM2 B1	13.50	53.81	336.7	33.0	9.0	nd	0.57	0.05	0.22	379.6
KM2 B2	13.55	54.02	329.4	33.6	9.7	nd	0.57	0.08	0.21	373.5
KM2 B3	13.65	46.95	457.1	33.5	7.7	nd	0.58	0.06	0.23	499.2
KM2 B4	14.50	44.35	439.5	28.6	7.1	nd	0.56	0.14	0.30	476.1
KM2 B7	16.08	44.35	516.0	27.8	6.9	nd	0.66	0.08	0.25	551.7
KM3										
KM3 B1	0.17	52.83	265.8	22.7	17.6	nd	0.51	0.52	nd	307.2
KM3 B2	0.54	54.23	366.9	22.3	21.7	nd	0.65	0.71	nd	412.2
KM3 B3	0.82	51.51	417.8	20.4	22.7	nd	0.84	1.76	nd	463.6
KM3 B4	1.52	55.95	8.9	25.2	33.4	3.63	0.13	0.00	0.21	71.5
KM3 B7	4.20	57.53	13.1	25.3	25.7	3.45	0.18	0.00	nd	67.7

nd = "not detected".

When compared with the data from the Upper Cretaceous Peripedhi Formation bentonite at the Parsata site in southern Cyprus [9], the ΣCEC values are very similar, as is the degree of loading with Ca > Mg > Na > K. The most significant difference is that Ca massively dominates the ΣCEC at KM, accounting for 80%–95% of the total load, compared with 27%–56% at the Parsata site.

A possible explanation is that the bentonite samples may contain a small amount of soluble gypsum, which would have dissolved during the exchangeable cation extraction, thereby contributing anomalously high Ca to the solutions that were analysed by ICP-AES. As noted in Section 4.1, such gypsum could have been introduced to the bentonite post-depositionally, for example during the Messinian Salinity Crisis. Indeed, the so-called Gypsum Canyon deposit in the overlying Kalavasos Formation is only some 3 km NE of the quarry site [57]. However, the SO_3 concentrations in the XRF analyses (Section 4.1) show no close relationship with the Ca concentration, suggesting that gypsum may not be the source of the high Ca levels.

A more likely reason is that source of the Ca is simply the overlying limestone and underlying pillow lavas which top the ophiolite immediately below the bentonite. The limestone formation can act as an aquifer in this area (but see the comments in Section 3.2), so long-term dissolution of the carbonate by groundwater could release Ca to solution and this could diffuse into the underlying bentonite over long time periods. Similarly, the underlying pillow lavas contain high pH groundwaters

enriched in Ca(OH)$_2$ which can also diffuse upwards into the bentonites (cf. results from the Parsata site in southern Cyprus [8]).

Finally, it is of note that, as in the Parsata study, there is no simple relationship between the CEC and mineralogy, so it is assumed that a range of minerals (and not just smectite) are involved, although it is likely that smectite is dominating the exchange reactions.

4.4.2. Methyl Blue Adsorption

The smectite content of samples from boreholes KM1, KM2 and KM3 were calculated on the basis of the adsorption of methyl blue and the results are presented in Supplementary Materials Section S4 and summarised in Figure 13. It can be seen that there is no significant trend with depth in the cores, although core KM3 is generally more enriched in smectite than core KM1, with the single sample from core KM2 lying somewhere between them.
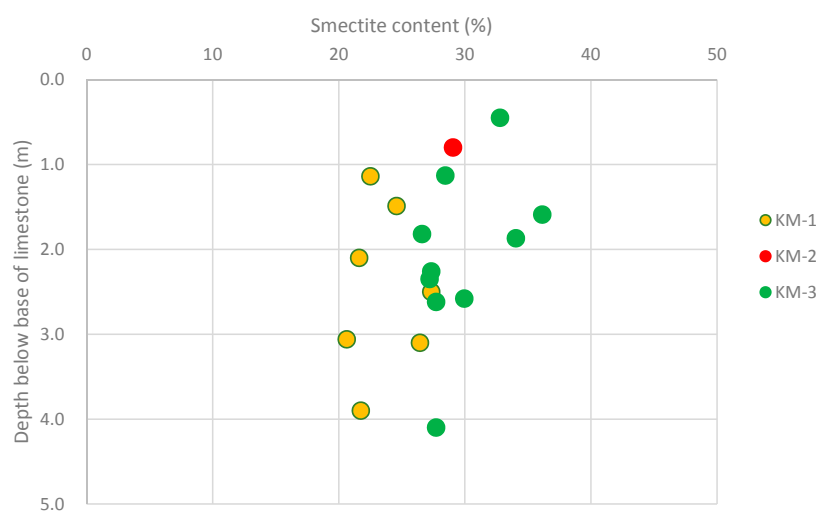

Figure 13. Calculated smectite content in samples from boreholes KM1, KM2 and KM3 versus depth below the base of the limestone overburden.

4.5. Stable Isotopes

Results of the δ^{13}C and δ^{18}O stable isotope analysis of limestone and carbonate mineralisation associated with the bentonite are shown in Table 7. These data are summarised in Figure 14, which presents a cross-plot of δ^{13}C and δ^{18}O and compares the data from the KM bentonite with the range of isotopic compositions found in normal marine limestones. This type of plot can be useful as a petrological tool to discriminate the genesis of carbonate mineralisation [58].

Table 7. δ^{13}C and δ^{18}O stable isotope values of carbonate minerals in the KM bentonites.

Sample	δ^{13}C	δ^{18}O
KM1 L1a	−7.48	−3.36
KM1 L1a2 (repeat analysis)	−7.71	−3.90
KM1 L1b	−7.57	−3.80
KM2 B5a	−6.29	−4.12
KM2 B5b	−6.76	−4.47
KM2 B7a	−6.20	−4.17
KM2 B7b	−6.12	−4.48
BDH calcium carbonate secondary standard (CCS)		
Measured value	−22.29	−13.24
Preferred value	−22.30	−13.35

The $\delta^{18}O$ composition of carbonate mineralisation depends principally on the oxygen isotope composition of the water from which it precipitates and the temperature which influences the isotopic fractionation of ^{18}O and ^{16}O between the water and carbonate mineral. Increasingly lighter oxygen (i.e., more negative $\delta^{18}O$) tend to be associated with decreasing salinity and progressively higher temperatures [58]. In contrast, the $\delta^{13}C$ composition of carbonate mineralisation is largely influenced by the isotopic composition of bicarbonate dissolved in the water. This will be controlled by different sources and processes that give rise to the formation of dissolved bicarbonate or dissolved carbon dioxide. For carbonates, the carbon and oxygen isotopic fractionation is commonly quoted relative to the Pee Dee Belemnite (PDB) standard. By definition, its isotopic composition is taken as $\delta^{13}C = 0$ and $\delta^{18}O = 0$. Consequently, most normal marine carbonates are close to these values. Typical $\delta^{13}C$ PDB compositions of common carbonate precipitates (based on overview from [58]) include:

- Normal marine seawater and limestone: $\delta^{13}C$ PDB ~0‰ ± 2‰.
- Marine shells: $\delta^{13}C$ PDB typically 0‰ ± 2‰.
- Bacterial sulphate-reduction and oxidadtion of sedimentary organic matter: $\delta^{13}C$ PDB typically between −8‰ and −32‰.
- Methane oxidation: $\delta^{13}C$ PDB typically less than −35‰.
- Fermentation: $\delta^{13}C$ PDB around +5‰ to +10‰.
- Soil carbonates $\delta^{13}C$ PDB are around −8‰ to −12‰.
- Meteoric cements $\delta^{13}C$ PDB are around: −4‰ to −15‰.

Figure 14 shows that both the limestone (sample KM1 L1) and the nodular carbonates concretions (samples KM2 B5 and KM2 B7) are significantly isotopically lighter, with respect to both $\delta^{13}C$ and $\delta^{18}O$, than expected for primary marine carbonate sediments.

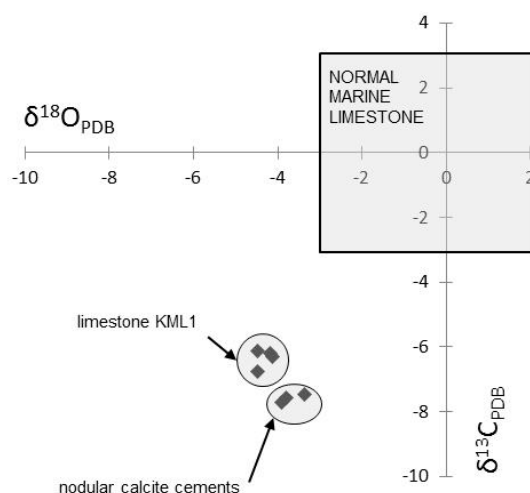**Figure 14.** Cross-plot of $\delta^{13}C$ and $\delta^{18}O$ summarising the stable isotopic composition of limestone matrix and authigenic calcite associated with the KM bentonite.

This indicates that calcite has been modified post-deposition as a result of burial diagenesis. The moderately light $\delta^{18}O$ values (−3.3‰ to −4.5‰) could be attributed to precipitation of secondary calcite or recrystallisation of primary micrite under slightly warmer conditions than most marine carbonate. The $\delta^{13}C$ values (−6‰ to −8‰) are similar to those expected from carbonate precipitation during bacterial sulphate reduction and oxidation of organic matter. The stable isotope signature of the nodular calcite concretions and the recrystallised limestone are similar to that found in many early burial cements and concretions [58]. These observations from a very limited suite of samples suggest that the KM bentonite sequence will have experienced at least a moderate degree of burial compaction and associated interaction with early diagenetic porewater.

4.6. Natural Decay Series (NDS)

The full results of the alpha- and gamma-spectroscopy analyses along with the activity ratios for ^{234}U/^{238}U, ^{230}Th/^{234}U, ^{230}Th/^{238}U and ^{226}Ra/^{230}Th for the KM quarry site samples are presented in Supplementary Materials Section S5. For the discussion of the NDS data, the main focus here is disequilibria in the activity ratios of the four main isotope pairs as this allows identification of both mechanisms involved along with timescales (see discussion in [59] for details).

In all three cores, the ^{234}U/^{238}U ratios are, within the uncertainty, all (apart from a few samples discussed below) at unity, indicating equilibrium conditions. The ^{230}Th/^{234}U ratios are all similarly at or near unity. Looking at the ^{226}Ra/^{230}Th ratios, it is clear that all samples are also at or near equilibrium, suggesting a non-disturbed system. However, as the analytical uncertainties are so large (due to the low activity concentrations of ^{226}Ra), it would be imprudent to make any further comment on these samples.

An useful method of presenting ^{238}U-^{234}U-^{230}Th data is in a plot of ^{234}U/^{238}U activity ratio against ^{230}Th/^{238}U activity ratio (Figure 15), which can be divided into U deposition and removal sectors corresponding to various continuous, sudden or complex processes (see [59,60] for discussion). Sample KM2-B7 lies in the U deposition sector, very close to the ^{234}U/^{238}U equilibrium line and so could have experienced deposition of U with ^{234}U in secular equilibrium with ^{238}U. Samples KM3-B2 and -B5 lie in the U removal sector (bottom half of the plot), but are so close to the equilibrium line that this suggests loss of ^{234}U in secular equilibrium with ^{238}U. All other samples plot in a position that could represent U loss in a single process on a timescale of the order of the ^{230}Th half-life (i.e., 7.54×10^4 years) although, within the analytical uncertainty, some samples plot in the complex processes sector.

However, it is worth noting that, in most cases, the ^{234}U/^{238}U activity ratios plot on or near the equilibrium line (within the analytical uncertainty) indicating that the U loss processes generally appear to feature movement of ^{234}U in secular equilibrium with ^{238}U.
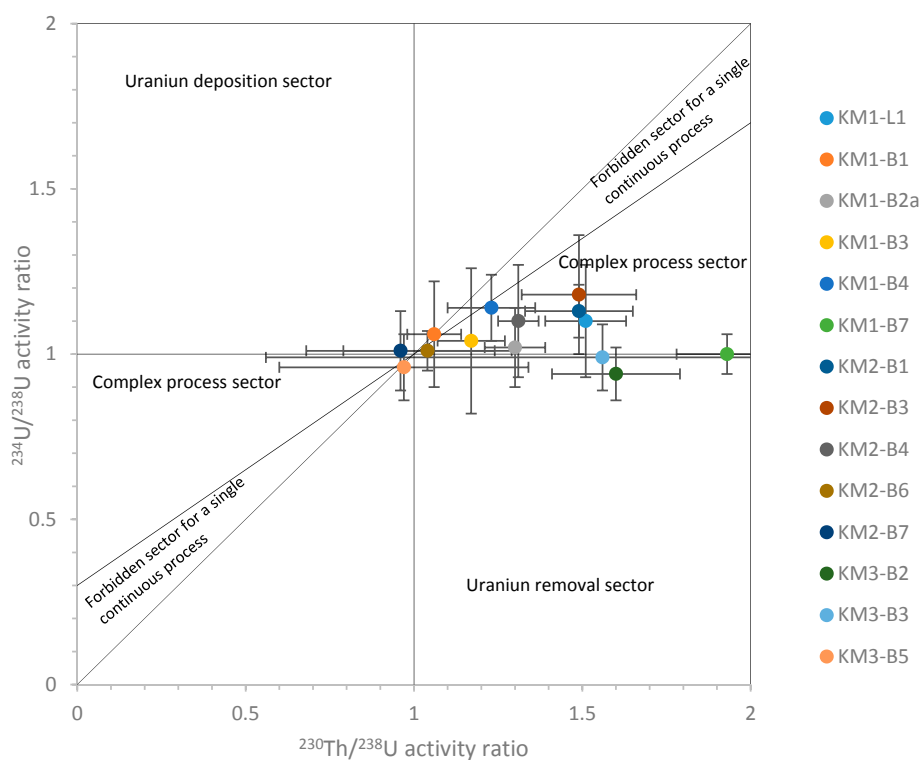

Figure 15. Plot of ^{234}U/^{238}U activity ratio against ^{230}Th/^{238}U activity ratio for samples from cores KM1, KM2 and KM3. NB 2σ uncertainty limits are shown due to the increased confidence level (95% compared to 68% for 1σ: see, for example, [61] for discussion).

5. Discussion

5.1. Repository Relevance

5.1.1. Site

The NA approach, namely using information from natural systems to assess the long-term behaviour of materials or processes assumed to occur in a repository, has been justifiably criticised in the past when the analogy between the natural system studied and the repository environment is weak or difficult to shown convincingly. As such, in this project, much effort was put into finding a repository-relevant site and numerous areas were examined across Cyprus before it was decided to focus on the Kato Moni (KM) quarry. As part of the study, a short geomorphological review of the site (set in the context of the entire island) indicated that the KM quarry site was ideal because:

- despite significant coupled uplift/erosion processes on the north side of the Troodos Massif producing massive sedimentary bodies and deep river valleys, the KM quarry ridge has likely been "protected" throughout much of this period (ca. 0.5 Ma) and has avoided catastrophic change.
- although the limestone overburden is an aquifer regionally, the isolated nature of the ridge suggests it has been uncoupled from the regional flow for some time, so minimising recent physico-chemical disturbance to the bentonite (something confirmed by the petrographic, stable isotope and NDS analyses).
- overall the climatic system in the area would tend to suggest that the site has been historically relatively dry, once again protecting the bentonite from significant external perturbations.

This is discussed further in Section 5.2, below.

5.1.2. Relevance to Expected Repository Behaviour

The fact that the bentonite overburden at the site is limestone, is highly appropriate as:

- the limestone density (wet density 2.2–2.45 Mg·cm^{-3}, dry density 2.01–2.31 Mg·cm^{-3}) is similar to that of concrete (e.g., SFR repository [62] concrete mould dry density 2.52 Mg·cm^{-3}, concrete tank dry density 2.67 Mg·cm^{-3}, NRVB grout [63] wet density 1.73 Mg·cm^{-3}, dry density 1.09 Mg·cm^{-3})
- many of the reactions between the limestone and the bentonite (e.g., diffusion of Ca into the clay from the limestone and pillow lavas) would also be expected between the concrete waste packages and waste forms and the bentonite in a repository
- Further, the petrographic data indicate there has been little or no reaction along the older fractures which are present in the bentonite, meaning the site is repository representative insofar that solute transport would appear to be dominated by diffusion
- The smectite content is particularly applicable to repository designs utilising lower quality bentonite or bentonite sand mixtures.

Timescales of reaction (i.e., loading) are difficult to ascertain at the moment as the palaeontological examination of the flora and fauna present in the rocks has proven inconclusive. Nevertheless, from a structural, tectonic and geomorphological perspective, it is expected that the bentonites are Late Eocene while the overlying limestones are Early Miocene and the palaeontological results obtained do not disagree with this viewpoint. As such, the period of bentonite loading comfortably exceeds any period of concern for a cementitious radioactive waste repository [8,64].

5.2. Bentonite Stability at Kato Moni

As the focus of this study is to assess evidence for creep in the bentonite (i.e., a physical process), it would be of use to discount any potential (hydro-geo-)chemical or thermal overprints on the bentonite. As noted in Section 4.5, the stable isotope data suggest that the bentonite has seen very little reaction

since the early diagenetic period following deposition. Further, the fact that the stable isotope signature of the limestone immediately overlying the bentonite is different to that observed in the bentonite, provides further indication of the basic imperviousness of the clays to outside change at this site—and lack of complicating factors for interpretation of the bentonite physical behaviour.

With respect to chemical impact, the NDS data (Section 4.6) indicate some movement of U in the system, most of which could be represented by equilibrium U loss in a single process on a timescale of the order of the ^{230}Th half-life (i.e., 7.54×10^4 years). Although there are indications of other disturbances in isolated samples (e.g., KM2-B7), the bentonite would otherwise appear to have been generally undisturbed since. Similarly, the CEC data (Section 4.4) indicate little change other than Ca dominance of the exchangeable ions (although this is still a minor proportion of the total Ca in the clays). While this exchangeable Ca may be from gypsum introduced to the bentonite post-depositionally (e.g., during the Messinian Salinity Crisis) a more likely source of the exchangeable Ca is simply the overlying limestone and underlying pillow lavas which top the ophiolite immediately below the bentonite. The limestone formation can act as an aquifer in this area, so long-term dissolution of the carbonate by groundwater could release Ca to solution and this could diffuse into the underlying bentonite over long time periods. Similarly, the underlying pillow lavas contain high pH groundwaters enriched in $Ca(OH)_2$ which can also diffuse upwards into the bentonites [9].

5.3. Bentonite Behaviour

As noted in Section 4.2.2., the bentonite samples from all three boreholes (KM1, KM2 and KM3) display micro-fracturing and micro-scale shear planes can be seen throughout the cores, being especially well-developed in the slightly coarser material. Unfortunately, it is not currently possible to define any sense in these structures and so no difference between load-induced, multi-directional shears and mono-directional, downslope shears can be identified for certain. However, multi-directional S- and C-type shears are present, clearly indicating movement in at least two directions, with the shear zone representing an accommodation of compressive stress by movement on foliation planes. This suggests they originate from loading due to the overlying limestones rather than gravitational tectonics (inducing slip into the neighbouring valleys).

KM3 appears to represent a more "micro-pellet" bentonite and this has had an impact on the shearing of the clay. In the pellet zone, anatomising shear plane networks are produced and this may prevent shear displacement to some degree. Certainly, "normal" shearing reappears at depth in KM3 in homogenous bentonite beneath the pellet zone.

Although the timescales of loading are not precisely known, it is assumed that the KM area has been above sea-level for <0.5 Ma and that, in that time, there has been (terrestrial) erosion of some ca. 25 m of overburden. As such, the loads are greater and the timescales longer than are of concern for a repository, but the KM bentonites show no significant deviation from "normal" natural bentonites. Indeed, as shown in Tables 4 and 5, the physical parameters of the KM bentonites are, aside from smectite contents which are lower than some repository bentonites, not dissimilar to those of industrial bentonites.

The Atterberg Limits (Table 4) define the ranges in moisture content that a bentonite will behave as a solid, plastic and liquid. The Liquid Limit (LL) of a bentonite is defined as the moisture content above which the material behaves as a liquid, and the Plastic Limit (PL) is the moisture content above which the bentonite behaves plastically. The numerical difference between the Liquid Limit and Plastic Limit is termed the Plasticity Index (PI)—see discussion in [65].

Of particular interest is the fact that the PL values are similar for all examples shown in Table 4 (with the KM bentonites being a little lower). For the KM samples, these values, when taken together with the Unconsolidated Undrained (UU) Triaxial Tests (carried out to obtain values of the cohesion and angle of shearing resistance, ϕ^o) data in Table 3, indicate that the natural bentonites lie in a region where shear could readily occur (see, for example [66,67]). Whilst the PL values for the industrial bentonites at emplacement in a repository lie in the same zone, Börgesson, L. et al. [7] note that

a sufficiently high swelling pressure should counteract this tendency. Their calculations for a SF repository design suggest that it is highly unlikely that such shear displacement will be an issue at the planned emplacement densities and full saturation (density at water saturation of between 1500 and 2000 kg·m^{-3} with associated swelling pressures of 0.08–7 MPa). More recent work [68,69] support the earlier results, but it should be noted that the studied shear values apply to "very high rates corresponding to the rates expected at a rock shear." [68] and so are not directly applicable to the situation expected in a repository for cementitious wastes.

As the final design for a cementitious waste repository which envisages a bentonite buffer around massive waste containers is yet to be finalised, the possibility of shear movement of the bentonite under load remains a process of interest. While various container designs exist, most are not designed to withstand the high external forces developed with fully saturated, high density bentonites. For example, Sakamoto, H. et al. [70] proposed a concrete canister which addressed the following design criteria:

- mechanical integrity and confinement of radioactivity in case of a drop accident during the interim storage phase
- degradation of concrete due to carbonation or ground water access
- confinement of radioactivity in the post closure phase
- performance in case of gas generation inside containers
- available experience with container type and materials
- costs

but did not touch on external confining pressures. Similarly, [63] noted that it is expected that the waste containers for the existing designs of shielded waste package will provide the waste package with adequate:

- mechanical strength to:

  - withstand stacking forces
  - resist damage due to pressurisation by internally generated gases
  - ensure that the specified impact accident performance can be achieved
  - withstand other loads that may occur during the long-term management of the waste package, as required by the generic Environmental Safety Case
- radiation shielding to ensure that the external dose rate is minimised and that the limits specified for transport are not exceeded
- thermal properties to ensure that the required fire accident performance and other requirements for the thermal performance of the waste package will be achieved
- resistance to degradation to ensure the overall integrity of the waste container is maintained for an adequate period.

Once again, no specific mention of external confining pressures. In addition, this SF design (in common with most SF and HLW repository designs) assumes full saturation of the bentonite to attain the high swelling pressures and evidence from URL experiments and natural bentonites [2,71] suggest that this will not happen in all cases.

6. Conclusions

When attempting to show the (close) relationship between engineered and natural barriers, it is worth remembering that one of the more important engineered barriers in a repository is not only directly derived from a natural material but, despite being processed to varying degrees, remains essentially the same material when emplaced in the repository. This being the case, the NA approach of comparing features, events and processes in the repository with analogous natural systems makes sense. Further, when providing reality checks for models which aim to assess the behaviour of engineered

barriers over repository-relevant timescales, the approach has clear benefits over short-term laboratory and URL experiments—although combining evidence from all three approaches is the only way to obtain comprehensive system understanding [16].

The work at the KM site has shown that both natural and industrial bentonites are intrinsically susceptible to shear, but it would appear that it may be possible to design around this susceptibility in certain repository designs for SF, an approach which may not be applicable to repositories for cementitious (L/ILW) wastes. For example, the high bentonite swelling pressures assumed in [7,68] are unreasonable in a cementitious waste repository as current waste package designs do not take this into account. In addition, this SF design assumes full saturation of the bentonite to attain the high swelling pressures and evidence from natural bentonites [2] suggest that this will not happen in all cases.

As such, open questions remain regarding the full significance of shear in bentonite and these could be addressed by limited further studies. For example:

- swelling pressures/density/Pl, etc., from a range of natural bentonites should be examined to assess the true impact of these parameters on bentonite shear for both L/ILW and SF repository designs. If full saturation cannot be automatically assumed, then models of bentonite shear such as [68] will need to be modified and the potential impact on the bentonite performance re-assessed.
- the sedimentary fabric impacts on the deformation and fracturing behaviour of the bentonite as, where banding or lamination is present, the bentonite displays intense micro-fracturing oriented parallel to the lamination. In addition, the shearing tends to be better developed in the slightly coarser material. This has implications for repository performance as, for example, in those concepts where pre-compressed bentonite blocks are foreseen—is there a difference in the fabric when uniaxially or triaxially compressed materials are employed?
- similarly with the disseminated shear in the parts of core KM3 which contain the pelletised bentonite, what does this imply for those design concepts which utilise bentonite pellets around waste packages?
- all three cores display shearing throughout, but it would be worth assessing if the smectite content has influenced the degree of shearing to any extent. As higher smectite content generally means higher plasticity, can any difference be seen between the lowest smectite containing samples in core KM1 (20.6% smectite) and the highest in core KM3 (36.2%)?
- that shear planes have been found throughout the natural bentonites at KM indicates that the basic conceptual model is correct, but without any sense of direction of these shears, these observations are of only limited value. As such, it is recommended that additional samples be collected at the KM site with a directional coring tool which will allow the sense of movement of the shears to be ascertained.
- it would be also advisable to drill deeper samples, down to the underlying pillow lavas, to obtain a better spatial understanding of the change in the internal structures of the bentonite with depth above the fixed boundary at the base of the bentonite.
- further examination of the "pellet" bentonite in the KM3 borehole would be useful as the inherited structure appears to spread the shear through anastomising shear plane networks, potentially minimising disruption of the bentonite fabric. This could be an alternative bentonite design option, so avoiding a potential redesign of existing waste containers.

Author Contributions: W. Russell Alexander and Heini M. Reijonen conceived and designed the experiment; W. Russell Alexander, Heini M. Reijonen and Andreas Siathas performed the field work; Gillian MacKinnon, Antoni E. Milodowski and Andreas Siathas analysed the samples; W. Russell Alexander, Gillian MacKinnon, Antoni E. Milodowski, Alistair F. Pitty, Heini M. Reijonen and Andreas Siathas interpreted the data; W. Russell Alexander and Heini M. Reijonen wrote the paper.

Conflicts of Interest: The authors declare no conflict of interest.

Abbreviations

The following abbreviations are used in this manuscript:

AFM	triaxial octahedral Al—Fe—Mg cations data plot
APFU	atoms per functional unit
BSEM	backscattered scanning electron microscopy
CEC	cation exchange capacity
EBS	engineered barrier system
EC	exchangeable cation
EDXA	energy-dispersive X-ray microanalysis
ESEM	environmental scanning electron microscopy
HLW	vitrified high-level waste
KM	Kato Moni
L/ILW	low- and intermediate-level waste
NA	natural analogues
NDS	natural decay series
PDB	Pee Dee Belemnite
PPL	plane-polarized light
SF	spent fuel
WOB	weight on bit
XPL	cross-polarized light

References

1. Alexander, W.R.; McKinley, L.E. *Deep Geological Disposal of Radioactive Wastes*; Elsevier: Amsterdam, The Netherlands, 2007.

2. Reijonen, H.M.; Alexander, W.R. Bentonite analogue research related to geological disposal of radioactive waste: Current status and future outlook. *Swiss J. Geosci.* **2015**, *108*, 101–110. [CrossRef]

3. Sidborn, M.; Marsic, N.; Crawford, J.; Joyce, S.; Hartley, L.; Idiart, A.; de Vries, L.M.; Maia, F.; Molinero, J.; Svensson, U.; et al. *Potential Alkaline Conditions for Deposition Holes of a Repository in Forsmark as a Consequence of OPC Grouting*; SKB R-12-17; Svensk Kärnbränslehantering AB (SKB): Stockholm, Sweden, 2014.

4. Alexander, W.R.; Reijonen, H.M.; McKinley, I.G. Natural analogues: studies of geological processes relevant to radioactive waste disposal in deep geological repositories. *Swiss J. Geosci.* **2015**, *108*, 75–100. [CrossRef]

5. Reijonen, H.M.; Alexander, W.R.; Marcos, N.; Lehtinen, A. Complementary considerations in Posiva's safety case: Support from natural analogues and natural systems. *Swiss J. Geosci.* **2015**, *108*, 111–120. [CrossRef]

6. Åkesson, M.; Kristensson, O.; Börgesson, L.; Dueck, A. *THM Modelling of Buffer, Backfill and Other System Components. Critical Processes and Scenarios*; SKB TR-10-11; Svensk Kärnbränslehantering AB (SKB): Stockholm, Sweden, 2010.

7. Börgesson, L.; Hernelind, J. *Canister Displacement in KBS-3V: A Theoretical Study*; SKB TR-06-04; Svensk Kärnbränslehantering AB (SKB): Stockholm, Sweden, 2006.

8. Svensk Kärnbränslehantering AB (SKB). *Barrier Process Report for the Safety Assessment SR-PSU*; SKB TR-14-04; Svensk Kärnbränslehantering AB (SKB): Stockholm, Sweden, 2014.

9. Alexander, W.R.; Milodowski, A.E. *Cyprus Natural Analogue Project (CNAP) Phase IV Final Report*; Posiva Working Report WR 2014-02; Posiva: Eurajoki, Finland, 2014.

10. Takaji, K.; Shigeno, Y.; Takafumi Shimogouchi, T.; Hirai, T.; Shiratake, T. *Improvement in Reliability of the Long-Term Mechanical Behaviour of Buffer Material*; Japan Atomic Energy Agency (JAEA): Tokai, Japan, 2005.

11. Petit, J.-C. Reasoning by analogy: Rational foundation of natural analogue studies. *Appl. Geochem.* **1992**, *7*, 9–12. [CrossRef]

12. Alexander, W.R.; McKinley, I.G.; Kawamura, H. The process of defining an optimal natural analogue programme to support national disposal programmes. In *Proceedings of the NEA-GRS Workshop on Natural Analogues for Safety Cases of Repositories in Rock Salt, Braunschweig, Germany, 4–6 September 2012*; Nuclear Energy Agency/Organisation for Economic Co-operation and Development (NEA/OECD): Paris, France, 2014; pp. 29–43.

13. McKinley, I.G. Applying natural analogues in predictive performance assessment (1): Principles and requirements; (2): Examples and discussions. In *Risk Analysis in Nuclear Waste Management*; Klewer Academic Publisher: Dordrecht, The Netherlands, 1989; pp. 357–396.

14. West, J.M.; Alexander, W.R.; Kaku, K.; McKinley, I.G.; Shimmura, A. Communication of nuclear power concepts to stakeholders. The use of Nature's own laboratories. In *Japan Atomic Energy Research Institute Report, Proceedings of the NUCEF 2001—Scientific Bases for Criticality Safety, Separation Process and Waste Disposal, Tokai, Japan, 31 October to 2 November 2001*; Japan Atomic Energy Research (JAEA): Tokai, Japan, 2002; pp. 47–54.

15. Alexander, W.R.; Arcilla, C.A.; McKinley, I.G.; Kawamura, H.; Takahashi, Y.; Aoki, K.; Miyoshi, S. A new natural analogue study of the interaction of low-alkali cement leachates and the bentonite buffer. *Sci. Basis Nucl. Waste Manag.* **2008**, *56*, 493–500.

16. Alexander, W.R.; Gautschi, A.; Zuidema, P. Thorough testing of performance assessment models: The necessary integration of in situ experiments, natural analogues and laboratory work. *Sci. Basis Nucl. Waste Manag.* **1998**, *21*, 1013–1014. [CrossRef]

17. Miller, W.M.; Alexander, W.R.; Chapman, N.A.; McKinley, I.G.; Smellie, J.A.T. *Geological Disposal of Radioactive Wastes and Natural Analogues*; Waste Management Series; Pergamon: Amsterdam, The Netherlands, 2000; Volume 2.

18. Smellie, J.A.T.; MacKenzie, A.B.; Scott, R.D. An analogue validation study of natural radionuclide migration in crystalline rocks using uranium series disequilibrium: preliminary results. *Sci. Basis Nucl. Waste Manag.* **1985**, *9*, 91–98. [CrossRef]

19. Japan Nuclear Cycle Development Institute (JNC). *H12: Second Progress Report on R&D for the Geological Disposal of HLW in Japan*; Japan Atomic Energy Agency (JAEA): Tokai, Japan, 2000.

20. Pate, S.M.; McKinley, I.G.; Alexander, W.R. *Use of Natural Analogue Test Cases to Evaluate a New Performance Assessment TDB*; CEC Report EUR15176EN; European Union (EU): Luxembourg, 1994.

21. Japan Nuclear Cycle Development Institute (JNC). *H17: Development and Management of the Technical Knowledge Base for the Geological Disposal of HLW—Knowledge Management Report*; Japan Atomic Energy Agency (JAEA): Tokai, Japan, 2005.

22. Georgiou, A.; Dörflinger, G. *Assessment of Groundwater Resources of Cyprus*; Report TCP/CYP/8921; Ministry of Agriculture, Natural Resources and Environment: Lefkosia, Cyprus, 2002.

23. McCallum, J.E.; Robertson, A.H.F. Sedimentology of two fan-delta systems in the Pliocene-Pleistocene of the Mesaoria Basin, Cyprus. *Sediment. Geol.* **1994**, *98*, 215–244. [CrossRef]

24. McCallum, J.E. Sedimentology and Tectonics of the Plio-Pleistocene of Cyprus. Ph.D. Thesis, University of Edinburgh, Edinburgh, UK, 1989.

25. Poole, A.J.; Robertson, A.H.F. Pleistocene fanglomerate deposition related to uplift of the Troodos ophiolite, Cyprus. *Proc. Ocean Drill. Prog. Sci. Results* **1989**, *160*, 545–566.

26. Kinnaird, T.C. Tectonic and Sedimentary Response to Oblique and Incipient Continental—Continental Collision the Easternmost Mediterranean (Cyprus). Ph.D. Thesis, University of Edinburgh, Edinburgh, UK, 2008.

27. Shuter, E.; Teasdale, W.E. *Application of Drilling, Coring and Sampling Techniques to Test Holes and Wells*; U.S. Geological Survey, Techniques of Water-Resources Investigations; U.S. Geological Survey (USGS): Renton, WA, USA, 1989.

28. Kunimaru, T.; Ota, K.; Alexander, W.R.; Yamamoto, H. *Hydrochemistry of the Groundwaters from JAEA's Horonobe URL: Data Freeze II—Preliminary Evaluation of Boreholes HDB1 to HDB8 and Field Manual for on-Site Practices*; JAEA Report 2011-010; Japan Atomic Energy Agency (JAEA): Tokai, Japan, 2011.

29. Ewy, R.T. Shale/claystone response to air and liquid exposure, and implications for handling, sampling and testing. *Int. J. Rock Mech. Min. Sci.* **2015**, *80*, 388–401. [CrossRef]

30. Japanese Industrial Standards Committee (JISC). *Japanese Industrial Standard K 0131—General Rules for X-ray Diffractometric Analysis*; JIS: Tokyo, Japan, 1996.

31.　Japanese Geotechnical Society (JGS). *Japanese Geotechnical Society 0251–2000—Method for Preparing Samples for Identifying Clay Minerals in Soils*; JGS: Tokyo, Japan, 2000.

32.　Cyprus Organisation for Standardisation (CYS). *Cyprus Analytical Standard CYS CEN ISO/TS 17892-2004/2014/2015*; CYS: Lefkosia, Cyprus, 2015.

33.　British Standards Institute (BSI). *Tests for Geometrical Properties of Aggregates. Assessment of Fines. Methylene Blue Test*; BSI EN 933-9 Part 9; BSI: London, UK, 2010.

34.　Cyprus Organisation for Standardisation (CYS). *Cyprus Analytical Standard CYS CEN ISO/TS 17892-1:2014*; CYS: Lefkosia, Cyprus, 2014.

35.　Cyprus Organisation for Standardisation (CYS). *Cyprus analytical standard CYS CEN ISO/TS 17892-3:2015*; CYS: Lefkosia, Cyprus, 2015.

36.　Cyprus Organisation for Standardisation (CYS). *Cyprus Analytical Standard CYS CEN ISO/TS 17892-2:2014*; CYS: Lefkosia, Cyprus, 2014.

37.　Cyprus Organisation for Standardisation (CYS). *Cyprus Analytical Standard CYS CEN ISO/TS 17892-12:2004*; CYS: Lefkosia, Cyprus, 2004.

38.　Cyprus Organisation for Standardisation (CYS). *Cyprus analytical standard CYS CEN ISO/TS 17892-7:2004*; CYS: Lefkosia, Cyprus, 2004.

39.　Cyprus Organisation for Standardisation (CYS). *Cyprus analytical standard CYS CEN ISO/TS 17892-8:2004*; CYS: Lefkosia, Cyprus, 2004.

40.　Cyprus Organisation for Standardisation (CYS). *Cyprus analytical standard CYS CEN ISO/TS 17892-5:2004*; CYS: Lefkosia, Cyprus, 2004.

41.　Amman, L.; Bergaya, F.; Lagaly, G. Determination of the cation exchange capacity of clays with copper complexes revisited. *Clay Miner.* **2005**, *40*, 441–453. [CrossRef]

42.　Bascomb, C.L. Rapid method for the determination of cation exchange capacity of calcareous and non-calcareous soils. *J. Sci. Food Agric.* **1964**, *15*, 821–823. [CrossRef]

43.　Gillespie, M.R.; Kemp, S.J.; Vickers, B.P.; Waters, C.; Gowing, C.J. *Cation-Exchange Capacity (CEC) of Selected Lithologies from England, Wales and Scotland*; Environment Agency R&D Technical Report; Environment Agency (EA): Bristol, UK, 2001.

44.　MacKenzie, A.B.; Scott, R.D.; Linsalata, P.; Miekeley, N.; de Jesus, H.C. Inter-laboratory comparison of analytical methods for the determination of natural series uranium and thorium isotopes in rock samples. *J. Radioanal. Nucl. Chem.* **1994**, *182*, 21–34. [CrossRef]

45.　Cyprus Organisation for Standardisation (CYS). *Cyprus Analytical Standard CYS EN 933-9 Part 9*; CYS: Lefkosia, Cyprus, 1998.

46.　Ota, K.; Alexander, W.R. *Development and Testing of Radionuclide Transport Models for Fractured Crystalline Rock—An Overview of the Nagra-JNC Radionuclide Retardation Programme*; JNC Technical Review No. 11; Japan Atomic Energy Agency (JAEA): Tokai, Japan, 2001.

47.　Milodowski, A.E.; Basahm, I.R.; Hyslop, E.K.; Pearce, J.M. *The Uranium Source-Term Mineralogy and Geochemistry at the Broubster Natural Analogue Site, Caithness*; British Geological Survey Technical Report; British Geological Survey: Keyworth, UK, 1989.

48.　Phillips, E.R.; Everest, J.; Reeves, J. Micromorphological evidence for subglacial multiphase sedimentation and deformation during over-pressurized fluid flow associated with hydrofracturing. *Boreas* **2013**, *42*, 395–427. [CrossRef]

49.　Alexander, W.R. The use of natural, industrial and archaeological analogues in support of the borehole sealing project (Phase 2—Year 2015–2016). In *Sealing Site Investigation Boreholes: Phase II Annual Report for 2015/2016*; Jefferies, N.L., Joyce, S., Tsitsopoulos, V., Alexander, W.R., Börgesson, L., Karnland, O., Sanden, T., Gaus, I., Vomvoris, S., Metcalfe, R., et al., Eds.; RWM Ltd. Report RWM/03/XYZ; RWM Ltd.: Harwell, UK, 2016, in press.

50.　Bossart, P.; Mazurek, M. *Grimsel Test Site: Structural Geology and Water Flow-Paths in the Migration Shear-Zone*; Nagra Technical Report NTB91-12; Nagra: Wettingen, Switzerland, 1991.

51.　Ahonen, L.; Korkeakoski, P.; Tiljander, M.; Kivikoski, H.; Laaksonen, R. *Quality Assurance of the Bentonite Material*; Posiva Working Report WR2008-33; Posiva: Eurajoki, Finland, 2008.

52.　Posiva. *Safety Case for the Disposal of Spent Nuclear Fuel at Olkiluoto—Description of the Disposal System 2012*; Posiva Report 2012-05; Posiva: Eurajoki, Finland, 2012.

53. Kiviranta, L.; Kumpulainen, S. *Quality Control and Characterization of Bentonite Materials*; Posiva Working Report WR 2011-84; Posiva: Eurajoki, Finland, 2011.

54. Naoi, Y.; Komine, H.; Yasuhara, K.; Murakami, S.; Momose, K.; Sakagami, T. Influence of Seawater on Swelling Characteristics of Bentonite Buffer Material. *J. Jpn. Soc. Civ. Eng.* **2005**, *785*, 39–49, (*in Japanese*). [CrossRef]

55. Central Research Institute of the Electric Power Industry, CRIEPI Report N50209, 2007. Available online: http://criepi.denken.or.jp/jp/kenkikaku/report/leaflet/N05029.pdf (accessed on 9 January 2017).

56. Wilson, J.; Savage, D.; Bond, A.; Watson, S.; Pusch, R.; Bennett, D. *Bentonite: A Review of Key Properties, Processes and Issues for Consideration in the UK Context*; Quintessa Report; Quintessa Ltd.: Henley-on-Thames, UK, 2011.

57. Dunn, A.L. Paleoenvironmental interpretation of the messinian Kalavasos Formation in Gypsum Canyon, Kato Moni, Cyprus. In Proceedings of the 9th Keck Research Symposium in Geology, Willamstown, MA, USA, 9–11 April 1996; pp. 213–216.

58. Hudson, J.D. Stable isotopes and limestone lithification. *J. Geol. Soc. Lond.* **1977**, *133*, 637–660. [CrossRef]

59. Scott, R.D.; MacKenzie, A.B.; Alexander, W.R. The interpretation of ^{238}U-^{234}U-^{230}Th-^{226}Ra disequilibria produced by rock-water interaction. *J. Geochem. Explor.* **1992**, *46*, 323–343. [CrossRef]

60. Thiel, K.; Vorwerk, R.; Saager, R.S.; Stupp, H.D. ^{235}U fission tracks and ^{238}U-series disequilibria as a means to study Recent mobilization of uranium in Archaean pyritic conglomerates. *Earth Planet. Sci. Lett.* **1983**, *65*, 249–262. [CrossRef]

61. Scott, E.M.; Cook, G.T.; Naysmith, P. Error and uncertainty in radiocarbon measurements. *Radiocarbon* **2007**, *49*, 427–440. [CrossRef]

62. Svensk Kärnbränslehantering AB (SKB). *Initial State Report for the Safety Assessment SR-PSU, Updated 2015-10*; SKB TR-14-02; SKB: Stockholm, Sweden, 2015.

63. Radioactive Waste Management (RWM) Ltd. *Geological Disposal. Guidance on the Application of the Waste Package: Specifications for Shielded Waste Packages*; RWM Report WPS/702/01; RWM Ltd.: Harwell, UK, 2014.

64. Japan Atomic Energy Research (JAEA). *Second Progress Report on R&D for TRU Waste Disposal in Japan*; JAEA Review; JAEA: Tokai, Japan, 2007.

65. Bain, J.A. A plasticity chart as an aid to the identification and assessment of industrial bentonites. *Clay Miner.* **1971**, *9*, 1–17. [CrossRef]

66. Voight, B. Correlation between Atterberg plasticity limits and residual strength of natural soils. *Geotechnique* **1973**, *23*, 265–267. [CrossRef]

67. Olson, R.E. Shearing strength of kaolinite, illite and montmorillonite. *J. Geotech. Div.* **1974**, 1215–1299. [CrossRef]

68. Börgesson, L.; Dueck, A.; Johannesson, L.-E. *Material Model for Shear of the Buffer—Evaluation of Laboratory Test Results*; SKB TR-06-04; Svensk Kärnbränslehantering AB (SKB): Stockholm, Sweden, 2010.

69. Dueck, A.; Börgesson, L.; Johannesson, L.-E. *Stress-Strain Relation of Bentonite at Undrained Shear—Laboratory Tests to Investigate the Influence of Material Composition and Test Technique*; SKB TR-10-31; Svensk Kärnbränslehantering AB (SKB): Stockholm, Sweden, 2010.

70. Sakamoto, H.; Asano, H.; Tunaboylu, K.; Mayer, G.; Klubertanz, G.; Kobayashi, S.; Komuro, T.; Wagner, E. Concrete containers for long-term storage and final disposal of TRU waste and long-lived ILW. In Proceedings of the Waste Management'03 Conference, Tucson, AZ, USA, 23–27 February 2003; Waste Management Symposia: Tempe, AZ, USA, 2003.

71. Villar, M.V. (Ed.) *FEBEX Project Final Report: Post-Mortem Bentonite Analysis*; Publicación Técnica 05-1/2006; Empresa Nacional de Residuos Radiactivos (ENRESA): Madrid, Spain, 2006.